# Quality, compatibility, and synergy analyses of global aerosol products derived from the advanced very high resolution radiometer and Total Ozone Mapping Spectrometer

Myeong-Jae Jeong and Zhanqing Li[1]

Department of Meteorology and Earth System Science Interdisciplinary Center, University of Maryland, College Park, Maryland, USA

Received 15 February 2004; revised 7 September 2004; accepted 11 October 2004; published 26 March 2005.

[1] A number of global aerosol products of varying quality, strengths, and weaknesses have been generated. Presented here are synthetic analyses with regard to the quality, compatibility, and synergy of two long-term global (1983–2000) aerosol products derived from the advanced very high resolution radiometer (AVHRR) and the Total Ozone Mapping Spectrometer (TOMS). Four essential aerosol parameters, namely, aerosol optical thickness (AOT) from AVHRR under the Global Aerosol Climatology Project (GACP), TOMS AOT, Ångström exponent (AE) from AVHRR, and TOMS aerosol index (AI) are analyzed together with various ancillary data sets on meteorological fields, ocean color, and ground-based AOT measurements. While the two satellite products reveal some common features, significant discrepancies exist. Reflectances measured at ultraviolet and visible wavelengths from the two sensors are incompatible in terms of the magnitude of AE computed from AOT derived from the two channels. The spatial distributions of the aerosol products from AVHRR and TOMS are complimentary in revealing different aspects of aerosol characteristics. In-depth analyses were carried out over several regions under the influence of different types of aerosols such as biomass burning, dust, sea salt, air pollution, and their mixtures. A classification algorithm was developed to identify dominant types of aerosols around the globe using aerosol products from the two instruments. Aerosol type information is used to develop and apply relationships between the AVHRR AOT and the TOMS AOT. The latter was used to extend the AOT at 0.55 μm over land around the globe. Comparisons of monthly mean AOTs with AERONET monthly mean AOTs showed a general agreement to within an estimated error range of $\pm 0.08 \pm 0.20\tau$. Finally, a comparison between the estimated AOT with Moderate Resolution Imaging Spectroradiometer (MODIS) AOT over land showed good agreement in terms of magnitude and seasonality, suggesting a means of bridging past and current AOT estimations.

**Citation:** Jeong, M.-J., and Z. Li (2005), Quality, compatibility, and synergy analyses of global aerosol products derived from the advanced very high resolution radiometer and Total Ozone Mapping Spectrometer, *J. Geophys. Res.*, *110*, D10S08, doi:10.1029/2004JD004647.

## 1. Introduction

[2] Aerosols have been widely recognized as a major source of uncertainties in climate change studies [*Intergovernmental Panel on Climate Change* (*IPCC*), 2001]. Satellites have played a vital role in understanding the effects of aerosol on Earth's climate [*Kaufman et al.*, 2002], thanks to ample data available from a wide range of satellite sensors and the rapid development in satellite remote sensing techniques [*King et al.*, 1999]. While extensive and reliable aerosol products have been generated from a suite of advanced instruments such as the Moderate Resolution Imaging Spectroradiometer (MODIS) [*Tanré et al.*, 1997; *Kaufman et al.*, 1997], the Multiangle Imaging Spectroradiometer (MISR) [*Kahn et al.*, 1998, 2001; *Martonchik et al.*, 1998], and the Polarization and Directionality of the Earth's Reflectances (POLDER) instrument [*Goloub et al.*, 1999; *Deuzé et al.*, 2000], these products alone cannot meet the needs of long-term climate change studies due to their short observation periods. In this regard, aerosol products derived from the advanced very high resolution radiometer (AVHRR) and the Total Ozone Mapping Spectrometer (TOMS) have the unique advantage of offering observations for more than two decades.

[3] The AVHRR has been most extensively employed for aerosol studies, from which many aerosol products

[1] Also affiliated with Institute of Atmospheric Physics, Chinese Academy of Sciences, Beijing, China.


0148-0227/05/2004JD004647$09.00

have been generated using dual-channel algorithms [e.g., *Higurashi and Nakajima*, 1999; *Mishchenko et al.*, 1999; *Ignatov and Stowe*, 2002a], as well as single-channel algorithms [*Rao et al.*, 1989; *Stowe et al.*, 1997; *Ignatov et al.*, 2004]. The dual-channel algorithms solve for two aerosol parameters (AOT and AE) simultaneously, whereas the third generation single-channel algorithm first estimates AOTs in individual channels, and subsequently estimates AE from the AOTs [*Ignatov et al.*, 2004]. Concerning the TOMS instrument, after its measurements were found to be sensitive to biomass burning smoke [*Hsu et al.*, 1996], two major aerosol products were developed: the aerosol index (AI) [*Herman et al.*, 1997] and the AOT at 0.38 μm [*Torres et al.*, 1998, 2002]. The long-term record of aerosols based on AVHRR and TOMS measurements has been well documented with distinctive features on a global scale [e.g., *Herman et al.*, 1997; *Torres et al.*, 2002; *Geogdzhayev et al.*, 2002; *Mishchenko et al.*, 2003; *Stowe et al.*, 2002].

[4] Despite the generally reasonable agreements reported between AOTs from satellites and ground-based measurements [*Ignatov et al.*, 1995; *Stowe et al.*, 1997; *Torres et al.*, 2002], these aerosol data suffer from numerous inherent shortcomings that have not been fully understood. Substantial differences were found among various satellite-based AOT estimates and in comparison with ground-based observations [*Myhre et al.*, 2004; *Kinne et al.*, 2001]. Part of the inconsistencies originate from the mismatch between the products, especially between satellite (areal mean) and surface point measurements due to spatial and temporal sampling differences [*Haywood et al.*, 2001; *Kinne et al.*, 2001]. Causes for the remaining inherent differences have yet to be identified and quantified.

[5] For global aerosol retrievals, various assumptions were made concerning the physical and/or optical characteristics of aerosols (e.g., spherical versus nonspherical particle shape, different refractive indices with wavelength dependencies, and various shapes and size distributions and vertical profiles) [*Mishchenko et al.*, 1995; *Tanré et al.*, 1997; *Kaufman et al.*, 1997; *Mishchenko et al.*, 2003]. Selection of an appropriate aerosol model is a major challenge, especially for global aerosol retrieval algorithms [*Nakajima et al.*, 1989; *Zhao et al.*, 2003] and can incur substantial discrepancies in the retrieval of aerosol optical depth [*Jeong et al.*, 2005]. It is contingent upon the knowledge of aerosol type, which may be better obtained from sensors with a suite of channels that span a proper range of the spectrum, or alternately from a combination of multiple satellite sensors.

[6] The AVHRR and TOMS aerosol products have their own advantages and disadvantages over each other. For example, the AVHRR products are limited to oceans due to difficulties in separating the signal of the aerosols from that of bright land surfaces [*Mishchenko et al.*, 1999], while TOMS can detect aerosols both over land and ocean except over the regions covered by snow/ice [*Herman et al.*, 1997; *Torres et al.*, 1998]. The TOMS aerosol products are affected by aerosol layer altitude and single-scattering albedo, and are more susceptible to subpixel cloud contamination due to its large footprint (about $40 \times 40$ km$^2$ at nadir) [*Herman et al.*, 1997; *Torres et al.*, 1998]. The TOMS aerosol data are thus derived from fewer samples than the AVHRR aerosol data. One may gain synergetic aerosol information by combining the two aerosol products. Few attempts have been made to improve aerosol characterization from multiple satellite sensors. *Cakmur et al.* [2001] used the TOMS AI and AOT from one-channel AVHRR retrievals to study the seasonal and interannual variability of dust aerosols. No such effort has been reported on a global scale. Analyses are also lacking toward revealing and understanding the discrepancies among various global aerosol products.

[7] This study attempts to (1) improve the understanding of aerosol characteristics regarding their spatial and temporal variations; (2) identify any common features and differences between the AVHRR and the TOMS aerosol products through comprehensive analyses of the products over some special regions of interest; and (3) explore and take advantage of any synergy existing between the two products for classifying aerosol types over global oceans and generate a global aerosol climatology over both ocean and land at a common wavelength (0.55 μm).

[8] The data sets employed are introduced in section 2. Regional characteristics and variations of the aerosol climatology are analyzed in section 3. Section 4 introduces the classification of aerosol types and the generation of an integrated aerosol product. Concluding remarks are given in section 5.

## 2. Data Sets

[9] An AVHRR-based aerosol product generated under the Global Aerosol Climatology Project (GACP) [*Mishchenko et al.*, 1999; *Geogdzhayev et al.*, 2002] (updated at http://gacp.giss.nasa.gov/) is employed in this study (hereinafter the product will be referred to as GACP/AVHRR or simply AVHRR product). It contains monthly mean AOT at 0.55 μm and AE from July 1983 through September 2001 over oceans. The product resolution is $1 \times 1$ degree in latitude and longitude. It was derived from clear-sky calibrated radiances from AVHRR channel 1 (nominal wavelength, $\lambda = 0.63$ μm) and channel 2 ($\lambda = 0.85$ μm) contained in the International Satellite Cloud Climatology Project (ISCCP) DX data set [*Rossow and Schiffer*, 1999]. The spatial resolution of the product is 30 km aggregated from AVHRR global area coverage (GAC) data with 4-km resolution sampled from the 1-km raw data. Aerosol particles are assumed to be homogeneous spheres with optical properties determined by the Lorenz-Mie theory. A modified power law size distribution was adopted with the aerosol refractive indices fixed as $m = 1.5 - 0.003i$. The shaping constant (i.e., the power exponent in the size distribution function), which is the parameter that determines the shape of the modified power law size distribution, has a unique relationship with the AE and the effective radius of aerosols.

[10] The performance of a dual-channel-based algorithm is expected to be superior to that of a single-channel algorithm in terms of information content [*Tanré et al.*, 1997; *Nakajima and Higurashi*, 1998; *Kahn et al.*, 1998; *Higurashi and Nakajima*, 1999] if the quality of both channels is similar. However, even in such cases, there are many sources of errors inhibiting accurate aerosol retrievals [*Ignatov et al.*, 1998; *Mishchenko et al.*, 1999]. Radiance calibration is one of the major uncertain factors [e.g.,

*Higurashi and Nakajima*, 1999; *Ignatov*, 2002], which could change the AOT by more than 40% [*Geogdzhayev et al.*, 2002]. Another major error source is cloud screening [*Ignatov and Nalli*, 2002; *Myhre et al.*, 2004]. In addition to the ISCCP cloud detection algorithm [*Rossow and Garder*, 1993], more conservative cloud screening algorithms were applied by *Mishchenko et al.* [1999] and *Geogdzhayev et al.* [2002]. The additional cloud screening aims to eliminate small cumulus clouds and optically thin cirrus clouds. However, strict cloud masking could have the adverse affect of discarding strong aerosol signals [*Husar et al.*, 1997; *Haywood et al.*, 2001]. Other possible error sources include the assumptions about aerosols (i.e., spherical particle, size distribution function and refractive indices) and boundary conditions (i.e., fixed wind speed and water-leaving radiance), and water vapor absorption at channel 2.

[11] In general, AE is known to be erroneous for small AOT (AOT < 0.2) [*Ignatov et al.*, 1998] and is related to the spectral separation between the channels [*Ignatov and Stowe*, 2002b]. Yet the accuracy of satellite-based AE is vulnerable to various uncertainties [*Ignatov and Stowe*, 2000; *Myhre et al.*, 2004]. *Ignatov* [2002] showed that the calibration gain is one of the most important factors hampering the retrieval accuracy of the AE, while *Geogdzhayev et al.* [2002] argued that uncertainties in the calibration intercept introduced an error in AE less than 0.4. Use of a long-term climatology can suppress random-like errors especially those associated with radiometric noise and digitization [*Ignatov et al.*, 1998; *Ignatov*, 2002].

[12] The TOMS aerosol products used here include the monthly mean AOT at 0.38 μm [*Torres et al.*, 1998, 2002] and the monthly AI (level 3, version 7) [*Herman et al.*, 1997]. They were inferred from TOMS measurements made by Nimbus-7 and Earth Probe from 1979 to 2000 (the AI data are archived at http://toms.gsfc.nasa.gov/). The TOMS AOT data have the same spatial resolution (1 × 1 degree) as the AVHRR data, while the TOMS AI data have a resolution 1 × 1.25 degree, but are interpolated to 1 × 1 degree grids. A temporal gap of three years exists between May 1993 and July 1996, mainly because the data from the METEOR-3 satellite were not used in aerosol data processing due to its precessing orbit [*Herman et al.*, 1997].

[13] The TOMS AI was calculated from the ratio of radiance measurements made at 340 and 380 nm. The index has the unique capability of differentiating between absorbing and nonabsorbing aerosols in the UV wavelengths over both oceans and land [*Hsu et al.*, 1996; *Herman et al.*, 1997] and even over very bright surfaces like clouds and ice/snow [*Hsu et al.*, 1999a]. Its sign is positive for absorbing aerosols such as mineral dust, biomass burning aerosols and volcanic ashes, and negative for nonabsorbing aerosols. The monthly mean data sets, however, were computed using only positive AI values. Any negative values were set to zero.

[14] A quantitative measure of aerosol load and AOT was also derived from TOMS [*Torres et al.*, 1998, 2002]. The TOMS AOT is most sensitive to aerosol absorption. The retrieval employed eight spherical aerosol models: one sulfate, three carbonaceous, and four dust models with a log normal size distribution and slightly wavelength-dependent refractive indices [*Torres et al.*, 2002]. The vertical distribution of aerosols was assumed to be a Gaussian distribution centered at 3 km for carbonaceous aerosols. For mineral dust, the climatological altitudes based on a chemical transport model [*Ginoux et al.*, 2001] were used. Both TOMS AOT and AI are sensitive to the altitude of the aerosol layer [*Hsu et al.*, 1999b]. An error of 2% in the AOT may result from an altitude error of 1 km for nonabsorbing aerosols and 65% for strongly absorbing aerosols [*Torres et al.*, 2002]. The TOMS AOT is relatively insensitive to the aerosol particle shapes (i.e., nonspheroid) due to the dominance of multiple molecular scattering in the near-ultraviolet (UV) region that weakens the effect of particle shape [*van de Hulst*, 1957].

[15] Subpixel cloud contamination is another major source of error that leads to overestimation of the TOMS AOT and is due to the large field of view of TOMS (40 × 40 $km^2$ at nadir). This effect is more significant for light loading of nonabsorbing aerosols. Fortunately, the bulk of absorbing aerosols are heavily loaded (e.g., dust storms and smoke plumes). The estimated overall uncertainty for the TOMS AOT is about 20% for nonabsorbing aerosols and 30% for moderately absorbing aerosols. A wrong choice of aerosol type can increase an AOT error by a factor of two [*Torres et al.*, 2002].

[16] Our analyses employed data that had all four aerosol parameters available. One year of data after the Mt. Pinatubo eruption (1991) were discarded in order to concentrate on tropospheric aerosols. So, the data periods of our study include July 1983 to June 1991, July 1992 to April 1993, and August 1996 to December 2000, with a total of approximately 13 years.

## 3. Regional Analyses of the Two Long-Term Aerosol Products

[17] The long-term averaged (1983–2000) seasonal maps of the four variables (i.e., GACP/AVHRR AOT and AE, TOMS AOT and AI) are presented in Figure 1 (only June, July, August (JJA) are shown). In general, the four products are complimentary to each other. For example, off the west coast of north Africa (10–25°N, 15–60°W; NW Africa), all products detected enhanced aerosol features simultaneously to a varying degree. For the AVHRR though, the continental source areas cannot be seen except for a large aerosol plume with a decreasing AOT gradient along the downwind direction indicating the source of aerosols (i.e., north Africa) that are clearly marked by the TOMS AOT and AI. However, the locations of the highest aerosol loading over land indicated by the TOMS AI and AOT are somewhat different from each other. The differences may stem from different treatments of cloud contamination. Since the TOMS AOT is more affected by residual clouds than the TOMS AI [*Herman et al.*, 1997], the former algorithm uses more strict cloud screening based on both AI and reflectivity thresholds [*Torres et al.*, 2002]. Consequently, their monthly products can originate from somewhat different samples.

[18] The TOMS AI is sensitive to both dust and smoke aerosols, although the sensitivity is higher for dust than for smoke [*Hsu et al.*, 1999b]. The combination of TOMS AI and AVHRR AE help differentiate the two types of aerosols. Optical properties of biomass burning aerosols are dominated by the accumulation mode [*Remer et al.*, 1998; *Eck et*

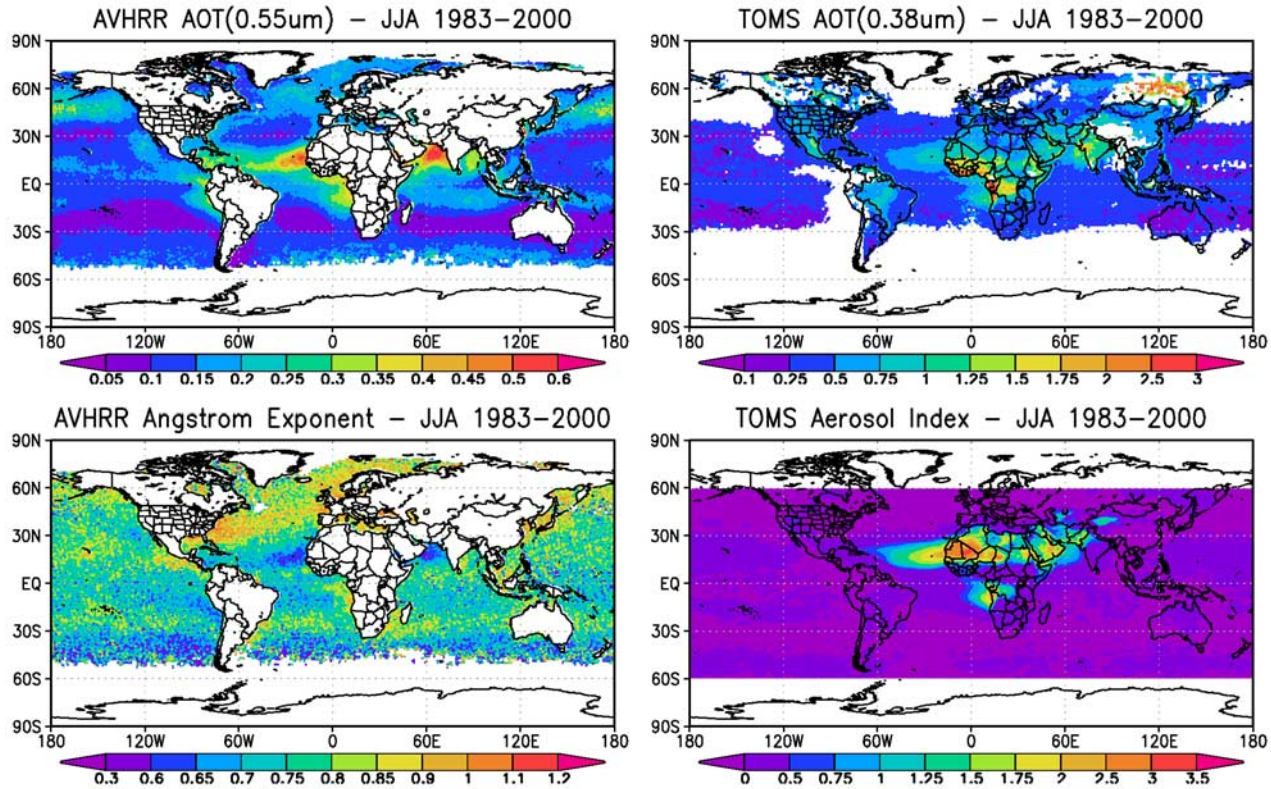


**Figure 1.** Long-term (1983–2000) seasonal mean global distributions of AVHRR AOT and AVHRR Ångström exponent (left panels) and TOMS AOT and TOMS AI (right panels).

*al.*, 1999] with the AE ranging from 1.0 to 2.3 [*Eck et al.*, 1999; *Dubovik et al.*, 2002], whereas those for dust are usually dictated by the coarse mode [*Eck et al.*, 1999; *Tanré et al.*, 2001] with a typical AE range of 0.1 to1.0 [*Eck et al.*, 1999; *Dubovik et al.*, 2002]. The generally low AVHRR AE around NW and west central (5°S–10°N, 35°W–10°E; WC Africa) African regions (exact locations vary with season) coincides with the enhanced TOMS AI and AOT, signifying the dominant dust aerosols there. A region off the southwest Africa (5–25°S, 15°W–15°E; SW Africa) is abundant in biomass burning aerosols [*Husar et al.*, 1997] whose seasonal occurrence and transport are discernable from the four aerosol products. During the months of JJA (Figure 1) and September, October, November (SON, not shown), for instance, all four variables are significantly high. This feature is not seen in other seasons, consistent with the finding that savanna and grassland fires generally occur from July to October [*Andreae et al.*, 1994; *Husar et al.*, 1997]. The Gulf of Guinea (i.e., WC Africa region) is affected by both biomass burning and dust [*Husar et al.*, 1997], which is echoed by relatively high AI and AOTs but intermediate AE.

[19] Clouds pose the most serious problem in satellite aerosol retrievals. They may exert influence in three ways: cloud contamination, misclassification of aerosol as cloud, and bias in data sampling due to the presence of clouds (no retrieval for cloudy pixels). Especially, heavy aerosol in the North Pacific Ocean (40–60°N, 150°E–150°W), the North Atlantic Ocean (30–60°N, 0–60°W), the eastern equatorial Pacific Ocean (0–20°N, 80–180°W; EC Pacific), and open oceans in the Southern Hemisphere midlatitudes (40–60°S) must be interpreted, or used, with caution, as they correspond to regions of extensive cloud cover. This is clearly seen from the JJA map of the ISCCP cloud fraction averaged from 1983–2000 [*Rossow and Schiffer*, 1999] (Figure 2). Almost all the regions of enhanced AOT coincide with high cloud fractions (>0.7). The distribution patterns of AVHRR AOT and ISCCP cloud fraction are so similar that this leads to a strong suspicion of cloud contamination, although one cannot rule out the possibility that aerosols are coincident with clouds. To gain further insight into the problem, regional analyses are presented below.

### 3.1. Peru Region

[20] Off the coast of Peru and Chile (10–30°S, 70–90°W) is a region of enhanced AOT (from the AVHRR) and cloud cover, small AE and zero AI. Adjacent to the South American continent, this region could be influenced by land sources of aerosol and the small AE might be a signal of dust aerosols transported westward from the Saharan desert. However, the AI value indicates little influence by any UV-absorbing aerosols (dust or biomass burning). Moreover, AERONET [*Holben et al.*, 1998, 2001] data collected at a few sites located upwind from Peru (e.g., Arica, Rio Branco, and Santiago, etc.) do not show the small AE values as obtained from the AVHRR. Yet, the seasonal variation of AE from AERONET is quite different from AVHRR, as seen in Figure 3. It shows the annual variations of daily AE measured at Arica (18.5S, 70.3W)

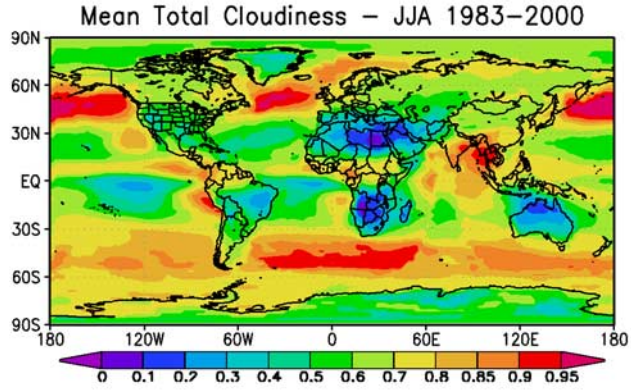


**Figure 2.** Seasonal mean cloud fraction from International Satellite Cloud Climatology Project (ISCCP) data for the same period as plots shown in Figure 1.

from 1999–2000 and long-term monthly means and standard deviations (STD) of AE from the AVHRR. Data from other nearby AERONET sites (not shown here) have even larger differences in terms of the seasonal variability. The incompatibility of AE attests to the possibility of cloud contamination of the AVHRR data, which is also supported by the correlations between the AVHRR AOT (and also the AE) and the spatial variability (STD) of the ISCCP cloud fraction (Figure 4). The STD was computed from cloud fractions within the Peru region and serve as a proxy of contamination by residual clouds. Cloud fraction itself may also serve as a proxy [*Ignatov and Nalli*, 2002]. However, we prefer to use STD since it is less affected by any bias

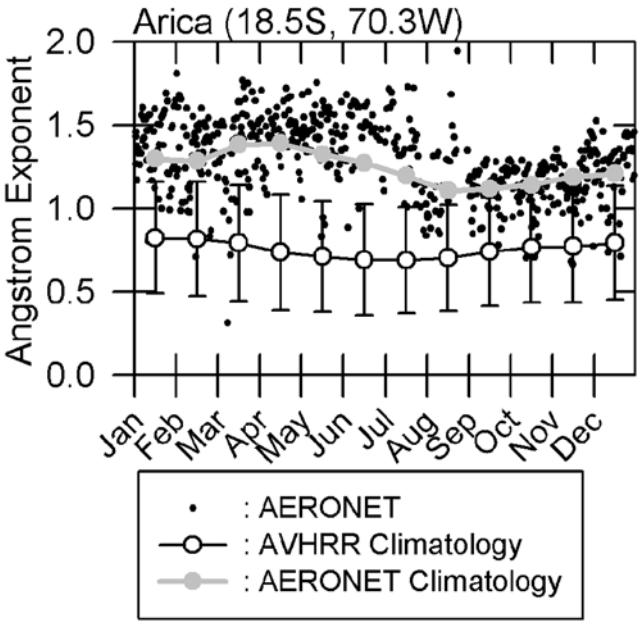


**Figure 3.** Annual variation of daily (small dots) and monthly (gray circles) Ångström exponents from an AERONET site (Arica, 1999–2000) and long-term (1983–2000) averaged AVHRR Ångström exponents (open circles) over the Peru region. Bars represent the standard deviation which contain the interannual variability.

existing in the ISCCP cloud fraction estimation. The STD was found to be positively correlated with the AOT and negatively correlated with the AE with the correlation coefficients equal to 0.62 and 0.73, respectively.

[21] Apart from cloud contamination, the region is likely to have a relatively high aerosol loading. Aerosol measurements during the East Pacific Investigation of Climate (EPIC) field experiment (September–October 2001) [*Bretherton et al.*, 2004] suggest that small particles from pollution sources along the Chilean coast and/or from local photochemical processes may be dominant in this region. *Kuang and Yung* [2000] reported the effects of anthropogenic sulfate aerosols in light of large $SO_2$ sources nearby and negative values of daily TOMS AI. Given various unusual features over this region, more detailed investigations are warranted to quantify the contributions of cloud contamination, local pollution and aerosol indirect effects, which may require in situ measurements.

### 3.2. Equatorial Regions

[22] The long plume of enhanced AOT in the equatorial eastern Pacific (0–20°N, 100–180°W; EC Pacific) is a common feature in satellite aerosol products [*Husar et al.*, 1997; *Myhre et al.*, 2004], but not in the results of aerosol transport models [*Chin et al.*, 2002] and model-satellite assimilations [*Yu et al.*, 2003]. Questions are thus raised if

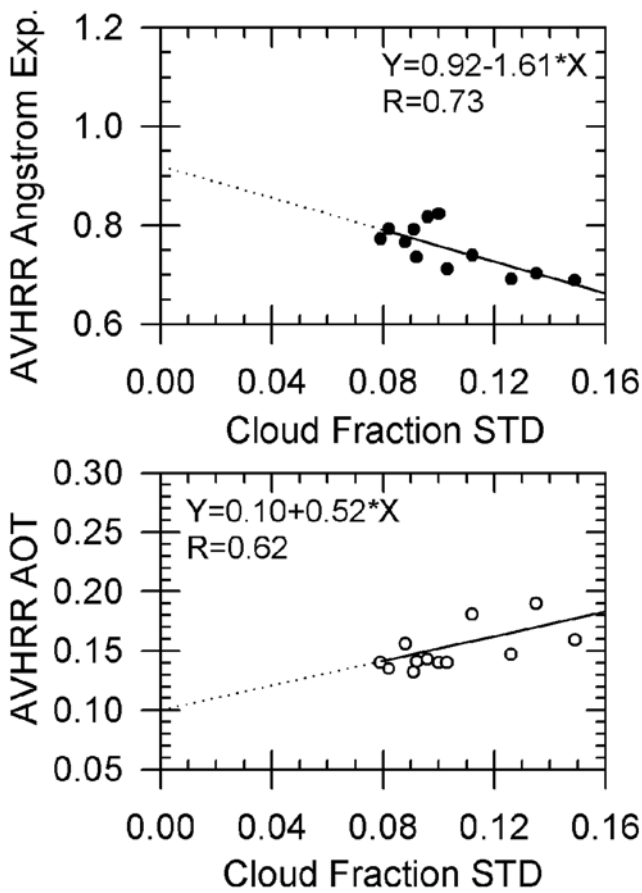


**Figure 4.** Ångström exponent and AOT as a function of standard deviation of the ISCCP cloud fraction. R is the correlation coefficient.

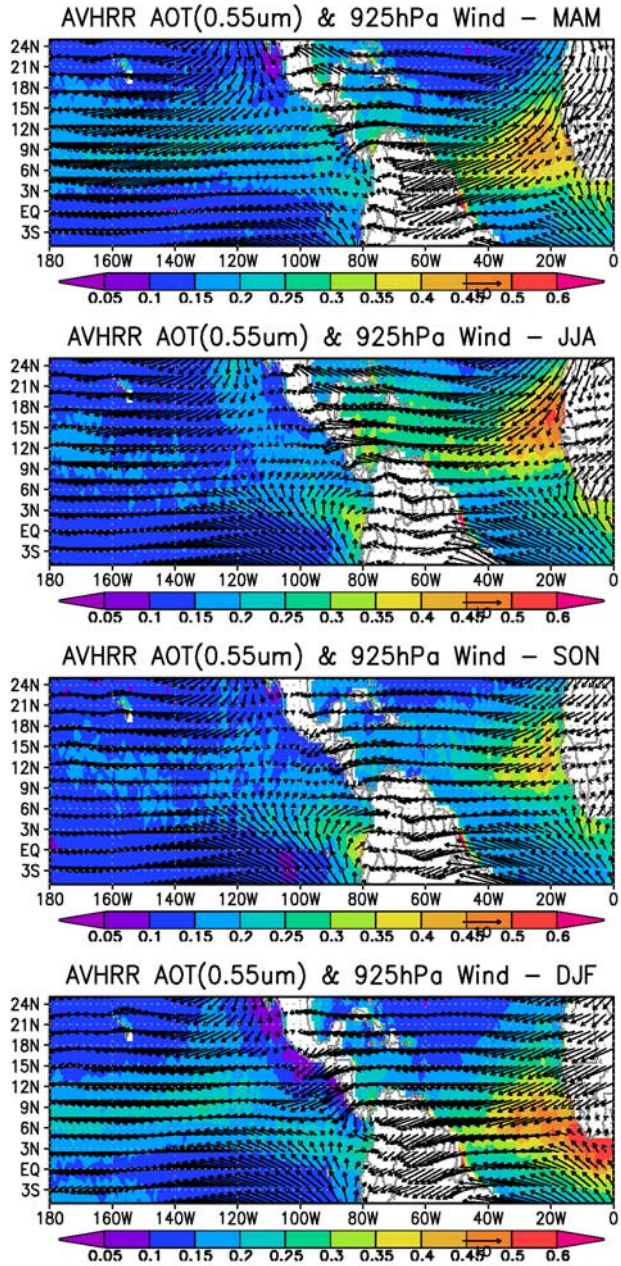


**Figure 5.** Seasonal mean AVHRR AOT around the equator in the Pacific and the Atlantic Oceans. Wind vectors at 925 hPa from NCEP/NCAR Reanalysis data sets are superimposed on the plots.

the feature is an artifact of the satellite products, and, if not, what are the causes for the plume. To address these questions, the AVHRR AOT is plotted over a large tropical domain for four seasons (Figure 5). Superimposed on the AOT map are the wind vectors from the National Centers for Environmental Prediction (NCEP) Reanalysis by the National Oceanic and Atmospheric Administration-Cooperative Institute for Research in Environmental Sciences (NOAA-CIRES) Climate Diagnostics Center (http://www.cdc.noaa.gov/). The patterns of the aerosol distribution are well correlated with low-level (e.g., 925 hPa) wind vectors, but not correlated with wind speeds at 1000 hPa (not shown here), suggesting a weak contribution of locally generated sea-salt aerosol. A visual examination of all individual monthly AOT and wind vector maps for 1983–2000 suggests that the long aerosol plume across the equatorial Pacific does not come from a single dominant source. It originates from Central America (during March, April, May (MAM) and JJA), the northern part of South America and north Africa (all seasons), as well as oceanic sources along the prevailing trade wind. The plume is located between the North Pacific and the South Pacific Highs, but its strength and pattern seem to vary with wind direction. The convergence of the trade winds in the north and south corresponds to the Intertropical Convergence Zone (ITCZ), but the plume does not exactly coincide with the ITCZ.

[23] The annual variations of the AVHRR AOT, AE, and the TOMS AOT are plotted for consecutive regions starting from the west coast of Africa through to the east Pacific oceans (Figure 6). The annual variations of AOT and AE are very similar in NW Africa, the Caribbean (10–25°N, 60–80°W), and Central America (10–25°N, 80–110°W) except during MAM in Central America. From NW Africa to Central America, the AOT decreases while the AE increases, indicating a decreasing influence of dust from Africa. The discordance during MAM for Central America is attributed in part to biomass burning which is active during this season and to local sources and transported pollutants [*Husar et al.*, 1997]. There are mixed signals of aerosols influencing the EC Pacific: the AVHRR AOT for EC Pacific is about the same or even greater than that for Central America in the upwind region; the pattern of the AE is similar to the Caribbean and NW Africa. There are two weak peaks in the TOMS AOT that are coincident with the biomass burning aerosol signal in Central America and the dust signal in the upwind regions. All these lead to the conclusion that biomass burning and dust affect the aerosol characteristics in the EC Pacific. Using a different AVHRR-based aerosol product based on a single-channel algorithm [*Stowe et al.*, 1997], *Husar et al.* [1997] argued that the region is influenced by non-sea-salt (nss) sulfates, Asian aerosols, and aerosols from volcanic activities, which is not obvious from this analysis.

[24] We thus make a hypothesis that the EC Pacific is likely influenced by various types of aerosols including sea salt, nss sulfate, dust and biomass burning aerosols, all depending upon the wind fields. Since some observations reported a weak seasonality in oceanic aerosols [*Husar et al.*, 1997], the seasonal changes revealed in this study attest to the contributions of aerosols from land sources.

### 3.3. North Pacific and Far East Asia Regions

[25] Many recent studies [e.g., *Husar et al.*, 2001; *Gong et al.*, 2003; *Zhang et al.*, 2003] dealt with the transport of Asian dust across the North Pacific. While the events were often detected from instantaneous AVHRR and TOMS data [*Herman et al.*, 1997; *Husar et al.*, 2001], the monthly data used here appear to indicate the dominance of small-sized aerosols even during MAM when Asian dust outbreaks occur. Figure 7 shows the distribution of the seasonal mean AVHRR AOT and AE across the North Pacific for MAM and JJA. Enhanced AOT (>0.2) spreads through almost the

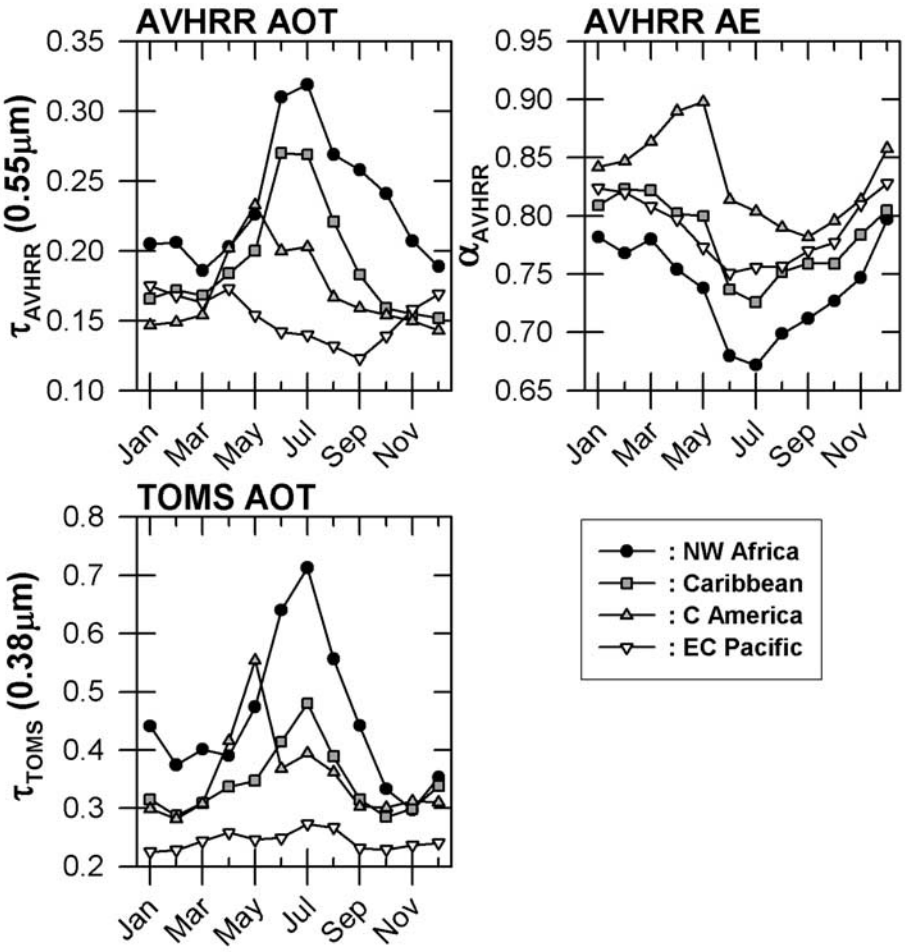


**Figure 6.** Long-term monthly mean AVHRR AOT, Ångström exponent, and TOMS AOT over NW Africa, Caribbean, Central America, and EC Pacific. Regions are as defined in the text. These regions are located next to each other along a latitudinal band.

entire region north of 30°N during MAM; it shrinks to a much smaller area during JJA and SON (not shown). However, the seasonal variation of the AE is much less marked, with slightly larger values during MAM and December, January, February (DJF; not shown) than during JJA and SON. This is contradictory to the seasonal trend of dust activities. Most likely, the magnitude of the seasonal change in the AE is less than its uncertainty. The lack of seasonal variation in the AE may have a physical reason. Unlike Saharan dust, Asian dust outbreaks are sporadic. Therefore, on a monthly timescale and on a 1 × 1 degree grid scale, averaging may smear out the signal of Asian dust. There are other possibilities. The dust events could be misclassified as clouds and removed [*Husar et al.*, 1997; *Haywood et al.*, 2001] and it may be that AE and AOT are contaminated by ocean color.

[26] To help reveal the sources (types) of aerosols that drive the seasonal and regional variations in the region, wind vectors at 925 hPa and 700 hPa from the NCEP/NCAR reanalysis are superimposed over the AVHRR AOT and AE maps, respectively, in Figure 7. A strong correlation is found between the AVHRR AOT and the wind direction, with all high (low) AOT corresponding to westerly (easterly) winds. During MAM and DJF, the westerly wind is dominant over the region such that aerosols from land sources (e.g., China, Korea and Japan) can be transported toward the east. The area of enhanced AOT also diminishes as the westerly wind retreats northward in JJA and SON. If this correlation is physically true, the enhanced AOT may be explained by fine-mode pollution aerosols generated in far east Asia, combined with background oceanic aerosols. In this case, the AOT is expected to decrease toward the Pacific, and the particle size (AE) is expected to increase (decrease) due to hygroscopic growth. This explanation seems to be corroborated with the regional variations of the AVHRR AOT and the AE plotted in Figure 8. It shows monthly AOT and AE at four regions located consecutively from west to east, namely, the Yellow Sea (25–45°N, 120–130°E), Japan (30–50°N, 130–145°E), NW (30–50°N, 145–180°E) and NE (30–50°N, 140–180°W) Pacific. Traces of Asian aerosols were observed over Midway Island and the Hawaii islands [*Prospero and Savoie*, 1989; *Prospero et al.*, 2003].

[27] An exception is noted in the middle of the Pacific where the AOT is high, especially during JJA. This points to another plausible cause, namely cloud contamination. The

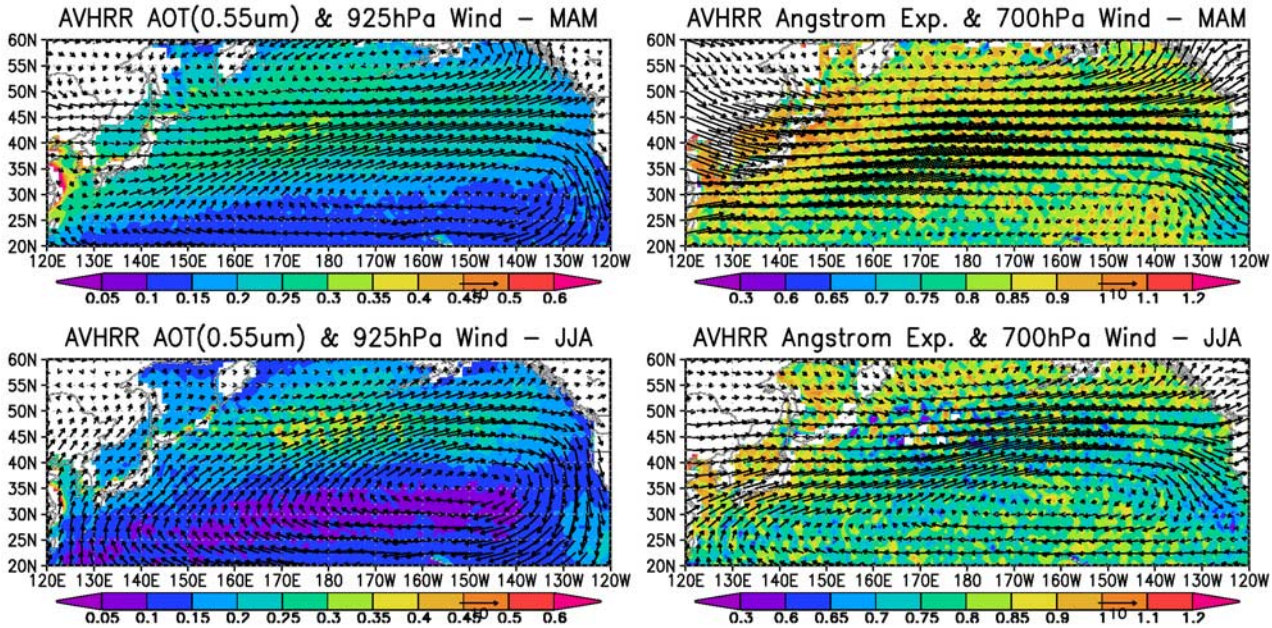


**Figure 7.** Seasonal mean (MAM and JJA) AVHRR AOT (left panels) and Ångström exponent (right panels) across the North Pacific Ocean. Wind vectors at 925 and 700 hPa from NCEP/NCAR Reanalysis data sets are superimposed on the AVHRR AOT and Ångström exponent plots, respectively.

left two panels in Figure 9 shows the ISCCP cloud cover distribution during JJA and MAM; the spatial pattern and temporal variation also bear a close resemblance to those of the AOT. Broadly speaking, a cloud cover of 0.7 (in yellow) seems to distinguish between AOT greater than and less than 0.2. There is a large area with cloud cover greater than 0.9 in the middle of the Pacific corresponding to the maximum in AOT. It is worth noting, however, that a large cloud cover does not necessarily lead to cloud contamination, which is dictated more by cloud scale than cloud cover frequency. Given that the presence of cloud in the region is controlled chiefly by large-scale frontal systems, the degree of cloud contamination should be less than in low-latitude regions. The relative uniformity and widespread extent of high AOT is more likely to be true in a qualitative sense, but a real challenge lies in quantifying the influence of cloud contamination on the satellite AOT retrievals.

[28] Another factor is associated with phytoplankton, which could contribute to high AOT and/or induce an artifact to cause false high AOT. Normally, a high chlorophyll concentration is found along the coastal regions and middle- and high-latitude oceans, as is shown in the right two panels in Figure 9 (shown only for MAM and JJA; data generated by a NOAA-NASA's Coastal Zone Color Scanner (CZCS) reanalysis (NCR) effort [*Gregg et al.*, 2002]). All these regions have high AOT. Figure 10 presents the correlation between long-term monthly mean AOT and the chlorophyll concentration in July over both the regions under study (the Yellow Sea, Japan, and NE/NW Pacific), as well as other regions of high chlorophyll concentration (N Atlantic, 35–50°N, 25–50°W; W Europe, 35–60°N, 0–25°W). Positive correlations are found in all regions. The correlation coefficients are larger than 0.5, except for Japan where the correlation is lowered due to a few cases of exceptionally high AOT corresponding to low chlorophyll concentrations.

[29] High phytoplankton concentrations can lead to formation of sulfate aerosols, which have important implications for climate [*Charlson et al.*, 1987]. Planktonic algae produce dimethylsulphide (DMS) and then, through oxidization, the DMS transforms into sulfate aerosols that are a major source of cloud condensation nuclei (CCN). It is, however, difficult to link this effect to the monthly satellite data, since the portion of such sulfate aerosols would be small compared to the total aerosol loading in the atmosphere. Besides, it is likely that the high AOT may be an artifact. Very high chlorophyll concentrations ($\geq$2.0 mg/m$^3$) and enhanced sedimentation can increase the water-leaving radiance in the visible spectrum [*Siegel et al.*, 2000]. Since the retrieval algorithm does not account for such changes,

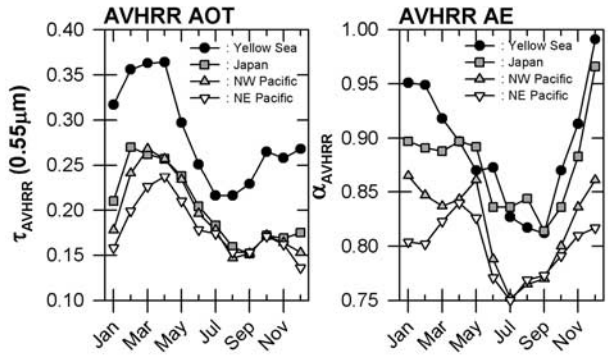


**Figure 8.** Long-term monthly mean AVHRR AOT and Ångström exponent over the Yellow Sea, Japan, NW Pacific, and NE Pacific.

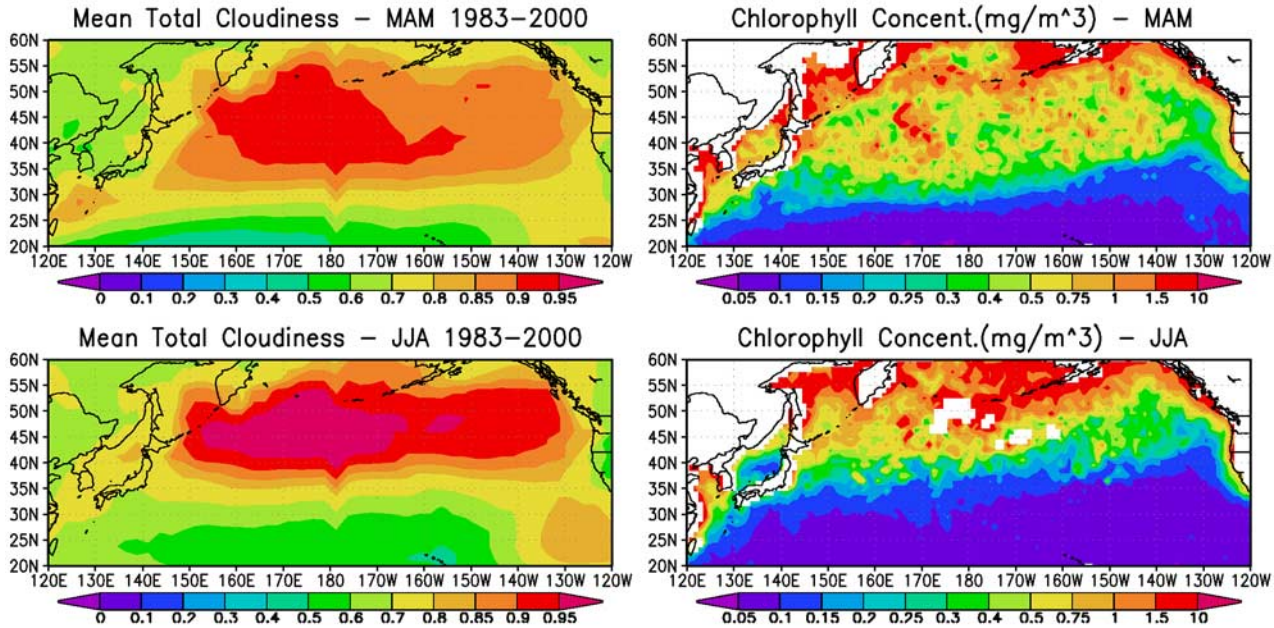


**Figure 9.** Seasonal mean cloud fraction (left panels; MAM and JJA, 1983–2000) from ISCCP data sets and seasonal mean chlorophyll concentration (right panels; MAM and JJA, 1978–1986) from NOAA-NASA's costal zone color scanner (CZCS) reanalysis (NCR) effort across the North Pacific Ocean.

the AOT may be overestimated. This is apparently the case for the sharp increase in AOT over a narrow strip along the east coast of China where ocean color is exceptionally bright due to sedimentation of very turbid water from the Yangtze River. The retrieval of ocean color (or chlorophyll concentration) and aerosol is often a convolved problem and thus becomes an obstacle in the retrieval of each other [e.g., *Fukushima and Toratani*, 1997]. Another challenge posed here is how to unravel their effects.

[30] We may thus make another conjecture that the lack of consideration of changes in ocean color may contribute to the spatial variation in AOT, but is unlikely to be the primary cause for the general trend of the AOT variation. So, again, the real challenges are (1) to quantify this

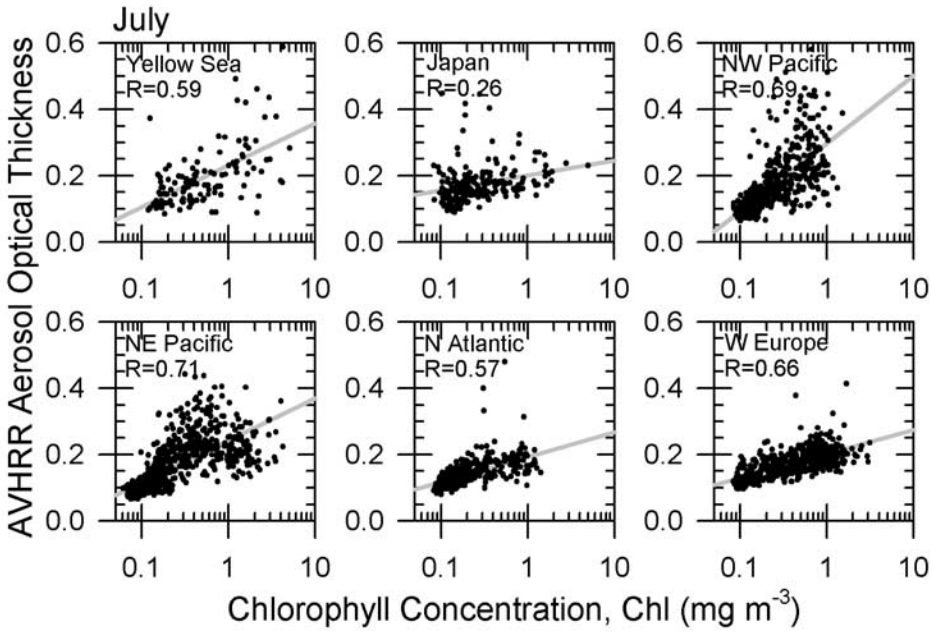


**Figure 10.** Long-term mean AVHRR AOT as a function of NCR chlorophyll concentration (Chl) over various regions in the North Pacific and North Atlantic Oceans. Solid gray lines represent the least-squared linear fit. R is the correlation coefficient.

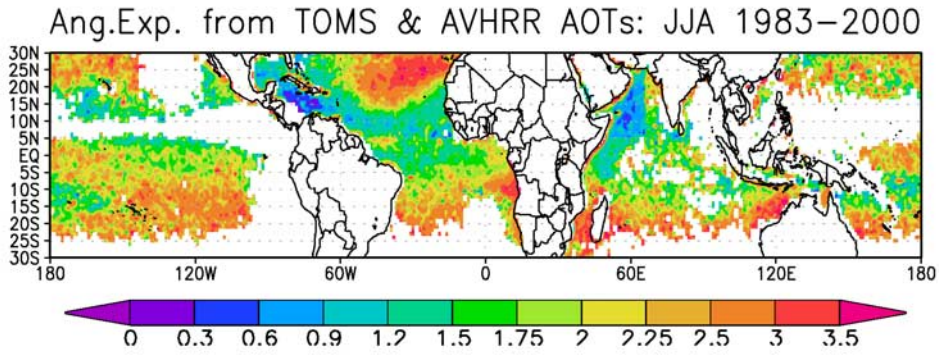


**Figure 11.** Ångström exponent derived from TOMS and AVHRR AOTs (JJA).

artificial effect, and (2) to establish a genuine physical relation between chlorophyll concentrations and oceanic aerosol loading. To this end, in situ measurements and modeling would be helpful. These issues will be addressed in future studies.

## 4. Synergy From AVHRR and TOMS Products

[31] It follows from the above analyses that the AVHRR and the TOMS do a reasonable job in retrieving AOT. However, they suffer from numerous problems, due to instrumental limitations and inversion difficulties. Note that neither of the instruments was optimized for aerosol studies. As each of the data sets has different advantages and shortcomings, the two may be combined to enrich aerosol information and to derive a synergetic product.

[32] One major difficulty in producing such synergy is that the TOMS and AVHRR retrievals typically have only a few days in common in each month and have different overpassing times, so that their individual monthly averages may have large uncertainties [*Cakmur et al.*, 2001]. As the uncertainties are largely random, they are suppressed by averaging [*Mishchenko et al.*, 1999]. As a measure of data compatibility, we first computed a test AE ($\alpha_{test}$) from the TOMS and AVHRR AOTs:

$$\alpha_{test} = -\ln\left(\tau^{TOMS}_{0.38\mu m}/\tau^{AVHRR}_{0.55\mu m}\right)/\ln(0.38\mu m/0.55\mu m). \quad (1)$$

Noting that the range of the AE due to the variability of aerosol properties is estimated to be 0–2 [*Kinne et al.*, 2001; *Dubovik et al.*, 2002], we can diagnose if the data sets are spectrally consistent by establishing whether $\alpha_{test}$ falls within a valid range of values. This has been proposed and used by *Ignatov and Nalli* [2002] for their AVHRR-based aerosol products. The estimates of $\alpha_{test}$ as computed by (1) contain both systematic and random errors. Systematic errors occur if the AOT from one sensor is systematically higher/lower than that of the other, out of a range expected for the channel difference. Random errors are primarily due to cloud contamination. *Myhre et al.* [2004] noted that the AOT from TOMS is systematically higher than that from AVHRR and further investigation into this discrepancy is presented later (section 4.2). If values of $\alpha_{test}$ are less than 0 or greater than 4, we deem them inconsistent and discard them. The test AE was calculated on different timescales: individual monthly means and seasonal means, and monthly and seasonal means averaged over the entire data period. 10% to 30% of the $\alpha_{test}$ computed from individual monthly AOTs fell within the range of abnormal values (i.e., $\alpha_{test} < 0$ or $\alpha_{test} > 4$). For the long-term averaged monthly and seasonal means, 2.6–3.8% and 2.1–2.6% of the $\alpha_{test}$, respectively, also fell within the range of abnormal values. Figure 11 shows the distribution of $\alpha_{test}$ calculated from the long-term mean AOT in JJA. The magnitude of $\alpha_{test}$ is systematically greater than the AVHRR AE except over major cloud regimes, while the gross pattern of distribution is similar to that of the AVHRR (see Figure 1). In terms of spatial distribution, most of the unreasonable $\alpha_{test}$ values reside in areas of low AOT for which the AE is very sensitive to errors in AOTs [*Ignatov et al.*, 1998; *Geogdzhayev et al.*, 2002], as well as regions with cloud contamination.

[33] These results suggest that AVHRR and TOMS AOTs do not have enough spectral consistency to be useful for extracting information concerning aerosol size due to differences in sampling and the magnitude/direction of their uncertainties. However, the distribution of $\alpha_{test}$ suggests that AVHRR and TOMS AOTs are correlated to each other geographically so are related to aerosol type. Any synergy existing between the two products should be exploited to help identify dominant aerosol types and to estimate AOT at one wavelength (AVHRR AOT) from the other (TOMS AOT).

### 4.1. Synergy 1: Identification of Aerosol Types

[34] Aerosol type information is crucial for many applications because different types of aerosols have distinct properties that may give rise to very different direct and indirect effects. Knowledge of aerosol type directly influences the quality of the AOT retrievals from satellite-measured radiances because the radiances are altered by both aerosol loading and aerosol optical properties. For global aerosol retrievals, several aerosol models are necessary to take into account highly variable aerosol characteristics [*Kaufman et al.*, 1997]. These aerosol models may be differentiated in terms of absorbing strength, particle shape, vertical distribution, etc. Currently, global distributions of aerosol type have been primarily derived through modeling [e.g., *Tegen et al.*, 1997; *Chin et al.*, 2002; *Penner et al.*, 2002, and references therein]. A handful of recent efforts focused on using satellite data to classify aerosol type on a

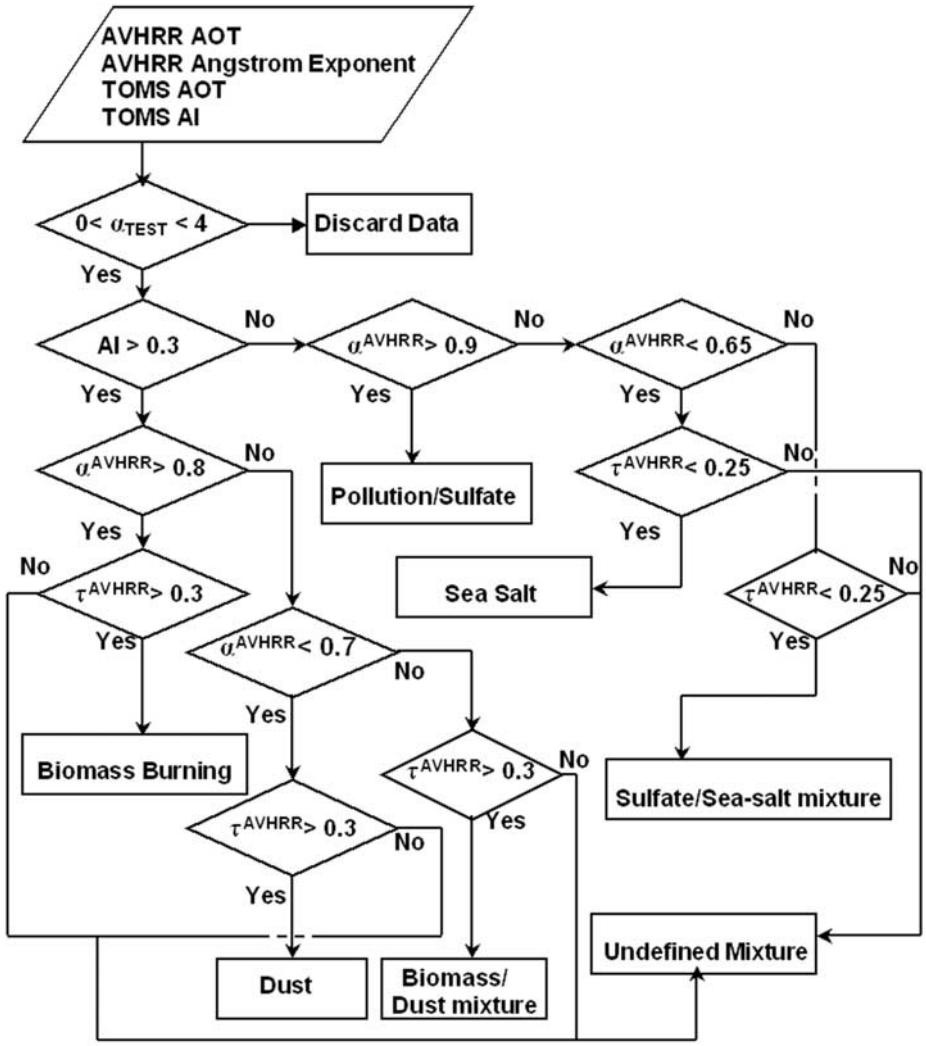


**Figure 12.** A classification algorithm for identification of dominant type(s) of aerosols.

global scale [*Kaufman et al.*, 2002]. By virtue of MISR multiangle observations, aerosols can be retrieved as mixtures of several components [*Martonchik et al.*, 1998; *Kahn et al.*, 2001]. *Bellouin et al.* [2003] attempted to separate dust, sea salt, and smaller-particle aerosols by utilizing the AOT and the AE from POLDER together with predefined aerosol regimes based on geographical location.

[35] While AVHRR data have been employed to extract aerosol size information and TOMS data have been used to measure aerosol absorption, the two data sets have not been combined to infer aerosol type. The analyses in section 3 demonstrated the utility of synchronizing the AVHRR AOT and AE and the TOMS AOT and AI to identify aerosol type. The algorithm is delineated in the flowchart shown in Figure 12. First, $\alpha_{test}$ (see equation (1)) is calculated from AVHRR and TOMS AOTs and only qualified data (i.e., $0 < \alpha_{test} < 4$) are employed. The TOMS AI can distinguish between UV-absorbing (biomass burning particles and dust) and non-UV-absorbing aerosols (sea salt, sulfate, pollution, etc.). Small (biomass burning particles, pollution, sulfates) and large (dust, sea salt) particles can be differentiated using the AVHRR AE. Intermediate values of the AE are assumed to represent mixtures of small and large particles. Numerous thresholds are applied to the AOT to refine the classification. For example, biomass burning, dust and some heavy pollution aerosols tend to have larger AOTs while the AOTs for light pollution (oceanic nss sulfate and sea salt) tend to be smaller. Some complicated mixtures of aerosols are designated as belonging to the "undefined" group, together with inconsistent data caused by data mismatch and cloud contamination. The threshold values are also given in the flowchart and were chosen based on aerosol climatologies derived from AVHRR and AERONET [*Dubovik et al.*, 2002].

[36] Figure 13 shows global seasonal maps of the dominant aerosol types classified by this algorithm. It captures well the seasonal and regional characteristics of the aerosols, as discussed in many other studies [e.g., *Husar et al.*, 1997; *Herman et al.*, 1997; *Torres et al.*, 2002]. As examples, one can find the pollution plumes over the midlatitude North Atlantic Ocean, far east Asia and the North Pacific, and dust and biomass burning aerosols from Africa. The colored areas over land indicates source areas for biomass burning and dust aerosols based on the values of the TOMS AOT (>1.0) and the AI (>1.25). The area with light pink over Russia during JJA represents aerosols from

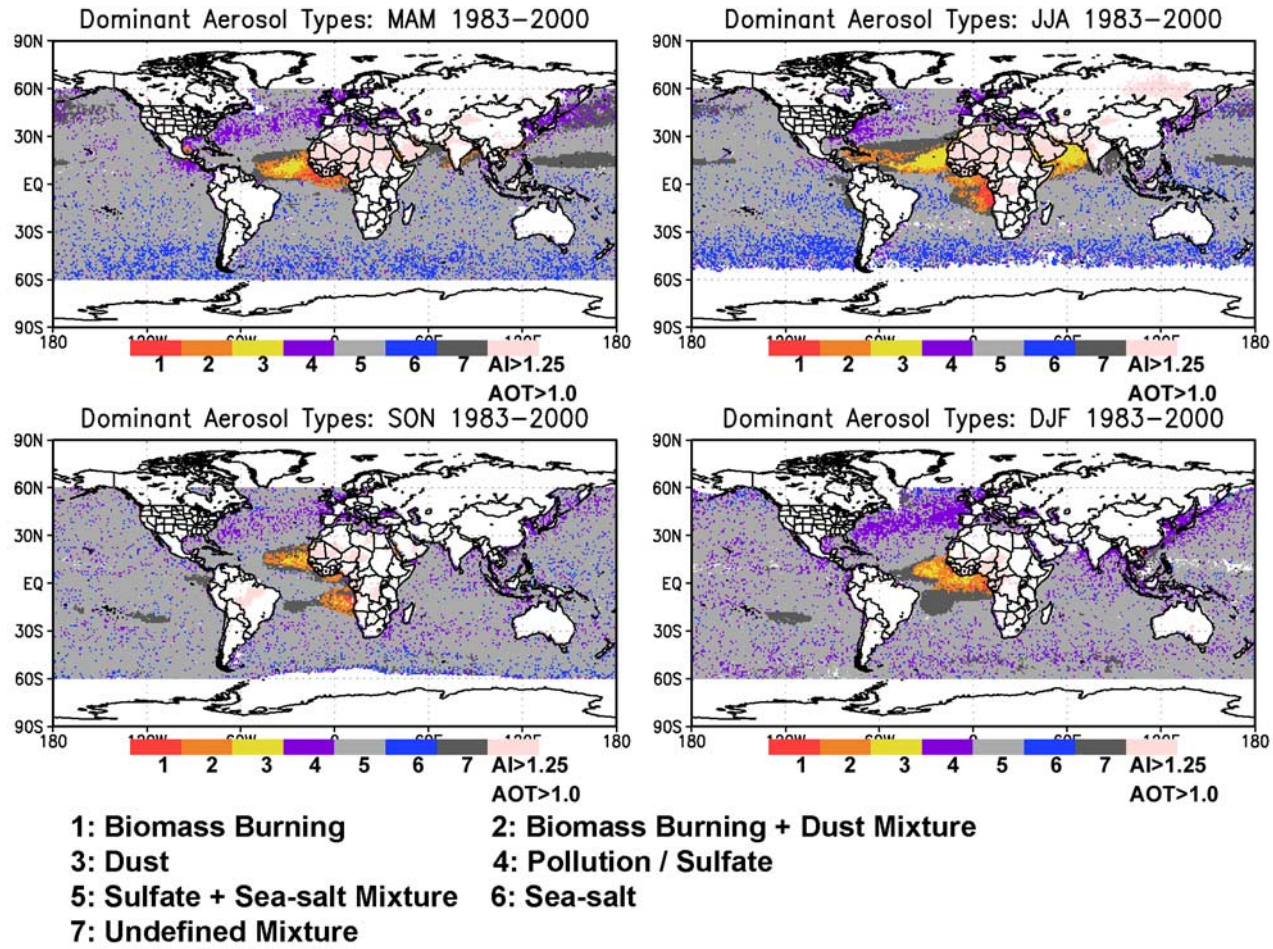


**Figure 13.** Global seasonal maps of dominant aerosol types based on the algorithm delineated in Figure 12. Land areas with TOMS AOT greater than 1 and AI greater than 1.25 are colored in light pink to indicate some major aerosol sources.

boreal fires as indicated by TOMS AOTs over a period of 1983–2000.

[37] The classification algorithm is flexible in that it can be adapted to any other data set containing similar information, although the threshold values may need adjustment. For instance, the AE is not an absolute measure of aerosol size and can vary with the wavelengths of the channels from which it is computed, and with physical/optical properties of aerosols. Thus its threshold may be tuned for different instruments and/or spatiotemporal resolutions. In addition, if a more robust physical parameter for aerosol size is available, such as the effective radius, better results may be acquired. For example, this algorithm could be applied to the MODIS and TOMS data sets. However, the Earth Probe/TOMS sensor's calibration problem since November 2000 (http://toms.gsfc.nasa.gov/aerosols/aerosols.html) may be a limiting factor. The algorithm would work better if data were from a single sensor or from sensors aboard a single satellite in order to avoid or lessen data mismatch problems.

[38] The algorithm has some limitations related to the appropriateness of the following assumptions: the characteristic size for each aerosol type, the capability of TOMS AI to discriminate UV-absorbing aerosols from non-UV-absorbing aerosols, and the consistency of data from different satellites. The performance of this algorithm is affected by the accuracy of the aerosol size parameter. Some aerosol events may possess particles with different size characteristics from those generally known, such as large biomass burning aerosols due to coagulation processes in thick smoke plumes [e.g., *Hobbs et al.*, 2003] or due to hygroscopic growth [e.g., *Zhou et al.*, 2002] and small to intermediate-sized marine boundary layer aerosols containing sea salt [*Murphy et al.*, 1998], to name a few. When data sets from different satellites are used, they may be derived from different scenes, in spite of the data consistency test procedures.

### 4.2. Synergy 2: Estimation of Global AOT at 0.55 μm

[39] It would be more useful to estimate the AOT at the same wavelength over both oceans and land so that one can identify more readily aerosol sources and their transportation. The AOT at 0.55 μm (or 0.5 μm) has been used as a common aerosol parameter in various studies [e.g., *Masuda et al.*, 1995; *Li and Moreau*, 1996]. An attempt is thus made here to generate a global integrated AOT product at 0.55 μm from AVHRR and TOMS instruments. This is achieved by

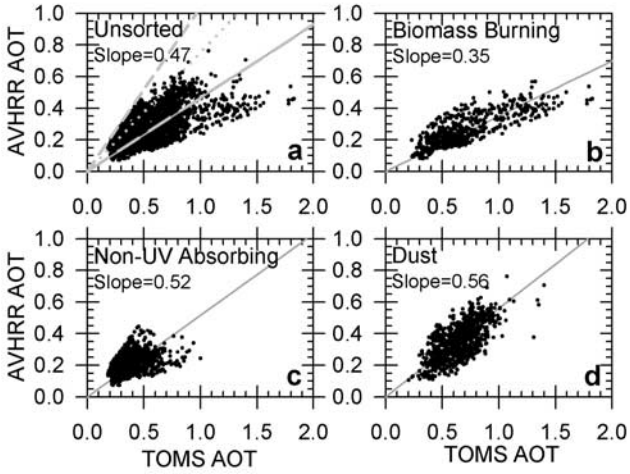


**Figure 14.** Scatterplots of TOMS AOT as a function of AVHRR AOT for various dominant types of aerosols. (a–d) Their linear regression lines are marked. In Figure 14a, modeled relationships are given for three dominant aerosol types as used in the TOMS aerosol algorithm: dust (medium-dash line), sulfate (short-dash line), and carbonaceous (long-dash line).

first developing regressional relationships between the AVHRR AOT and the TOMS AOT over oceans where both products are simultaneously available. To reduce random errors, the long-term (1983–2000) monthly averages are used. Figure 14a shows the relationship for biomass burning aerosols, dust aerosols and non-UV-absorbing aerosols. Overall, the TOMS AOT is systematically and significantly larger than the AVHRR AOT by a factor of approximately 2. Part of the difference is caused by the wavelength difference between the two channels (0.55 μm versus 0.38 μm), as is shown by three simulated relationships for dust, sulfate and carbonaceous model aerosols employed in the TOMS AOT retrieval [*Torres et al.*, 2002]. As is expected, larger differences correspond to finer aerosol particles. While the three lines are located among the observed data points, they are also all above the regression lines, implying that the AOT differences exceed the spectral dependence. It can thus be concluded that one product is over- (under-) estimated relative to the other. Such systematic differences are better accounted for by sorting the data according to aerosol type, as is shown in Figures 14b–14d. After data sorting, the two types of AOT have linear relationships whose slopes vary with aerosol type. Note that the intercept was set to zero in the regression. The difference diminishes to a factor of 1.7 for dust aerosols. We can use the relationship to estimate the AVHRR AOT from the TOMS AOT, or vice versa. The overall error range of estimation is $\pm 0.08 \pm 0.20\tau$, within which more than 95% of the data points reside.

[40] Without sorting the data according to aerosol type, *Myhre et al.* [2004] argued that the overall substantial scattering in the data results from differences in data sampling and cloud screening. We agree that part of this scattering is related to cloud and data sampling but this scatter can be reduced after sorting the data into different aerosol types. Another contributing factor lies in the use of different aerosol models in the retrieval algorithms. *Jeong et al.* [2005] demonstrated that considerable discrepancies between the AOT estimated from AVHRR and MODIS are attributed to differences in aerosol size distributions, namely, the power law (AVHRR) and (bimodal) log normal (MODIS) functions. Since the TOMS AOT is based on the log normal size distribution, similar discrepancies may also exist between TOMS and AVHRR. Large scattering is expected for non-UV-absorbing aerosols and low aerosol loading to which TOMS is rather insensitive.

[41] The AOT at 0.55 μm over land was obtained by applying the derived regression equations to the TOMS AOT, together with the AI and land cover data from the International Satellite Land Surface Climatology Project (ISLSCP; *Meeson et al.* [1995]). Owing to a lack of dynamic knowledge of aerosol types over land, the latter two data sets were used to grossly separate the data into smoke, dust and non-UV-absorbing aerosols. The AI was first used to group aerosols into UV-absorbing and non-absorbing aerosols. Absorbing aerosols are then classified as dust or biomass burning aerosols, depending if it is over vegetated or barren land. This simple assumption was made out of necessity. The maximum range of error due to this assumption is ±0.21*[TOMS AOT], when biomass burning was mistakenly selected instead of dust, or vice versa. However, this type of error is not a major factor according to comparisons against MODIS AOT as shown in the following discussions. The ensuing land AOTs are combined with the AVHRR AOTs over ocean to form a global climatology whose long-term average (1983–2000) is presented in Figure 15. It is seen that there is no artificial discontinuity between ocean and land and the map provides certain information pertaining to aerosol sources and transport.

[42] The estimated AOT over land are compared against monthly mean AERONET measurements (Figure 16). The best results are achieved in the Arabian region (Solar Village and Bahrain) followed by the South African region, with small random errors and little or no bias. Almost all data points fall within the range of estimated errors marked by the dashed lines. Larger scatterings exist for other locations, which is partially due to sampling errors in point specific measurements [*Kinne et al.*, 2001] and unexplained variability by the regression equations, as well as errors in the TOMS AOT data. There is a slight underestimation of the AOT in north Africa and an overestimation of the AOT in South America, but the bias errors in general are very small. While aerosols in both South Africa and South America stem from biomass burning, one reason for the better agreement in the former region is because the data used for developing the regression for biomass burning came from the region off the west coast of South Africa. The use of geographic location to select a regression equation can introduce errors especially for mixtures of dust and biomass burning aerosols in the Sahel region. Despite the numerous errors, most (~70%) of the estimated AOT reside within the estimated error range, when compared against AERONET data.

[43] The MODIS AOT data (April 2000 to March 2004) at 0.55μm over land are compared with our results. Since the overlapping period is short (less than a year), the comparison is performed for their respective long-term

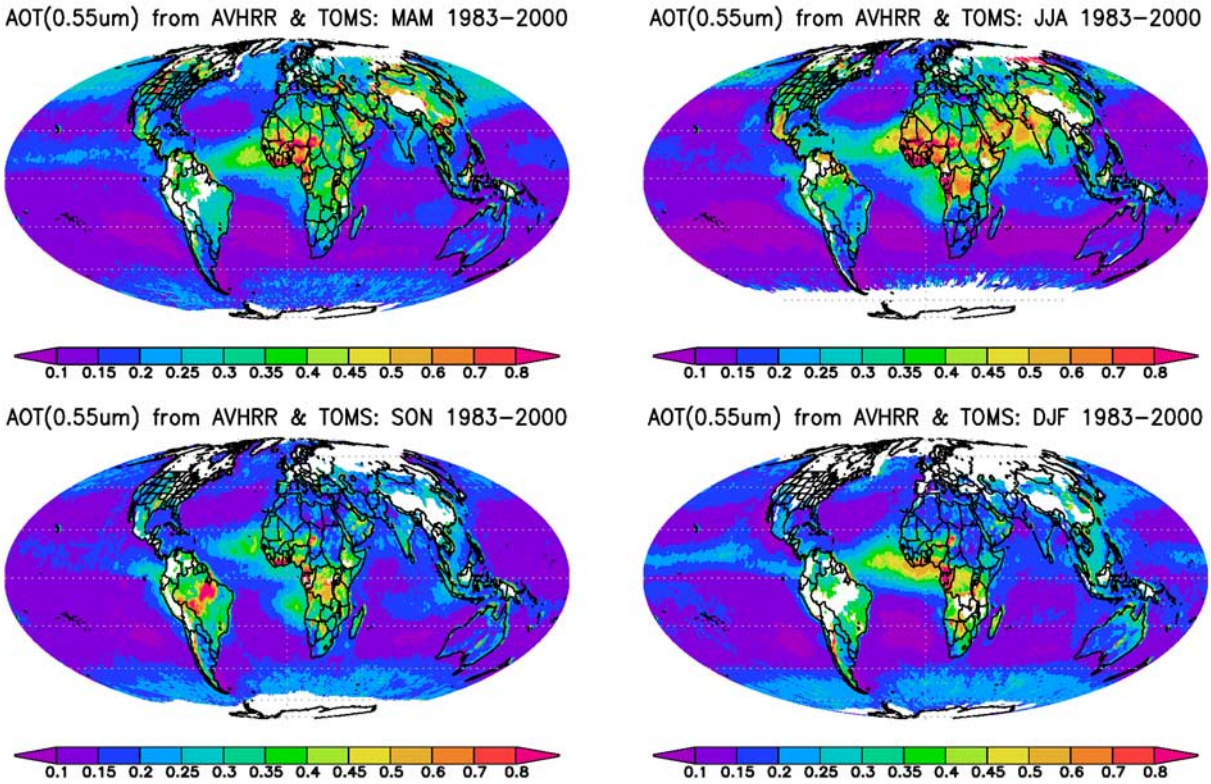


**Figure 15.** Global maps of seasonal mean AOT at 0.55 μm. AOT over land was estimated from regression equations on the basis of relationships among TOMS AOT and AI and AVHRR AOT. AOT over ocean is the AVHRR AOT as originally reported.

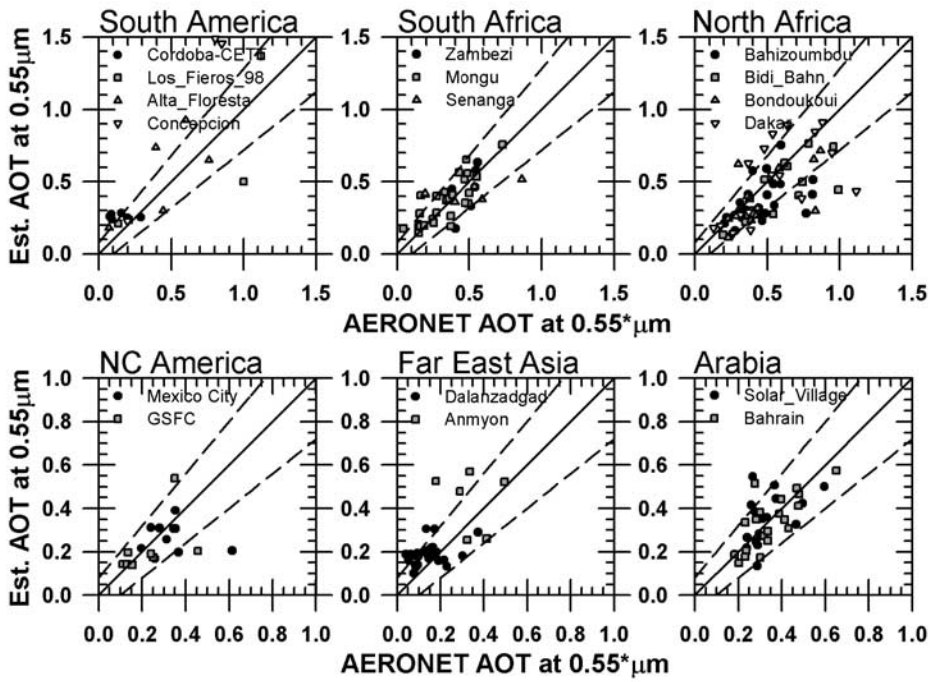


**Figure 16.** Comparison of estimated AOT over land against monthly AERONET AOT at 0.55 μm. AERONET AOT was interpolated using the Ångström exponent. The solid line is the one-to-one line, and the dashed line denotes the estimated error range.

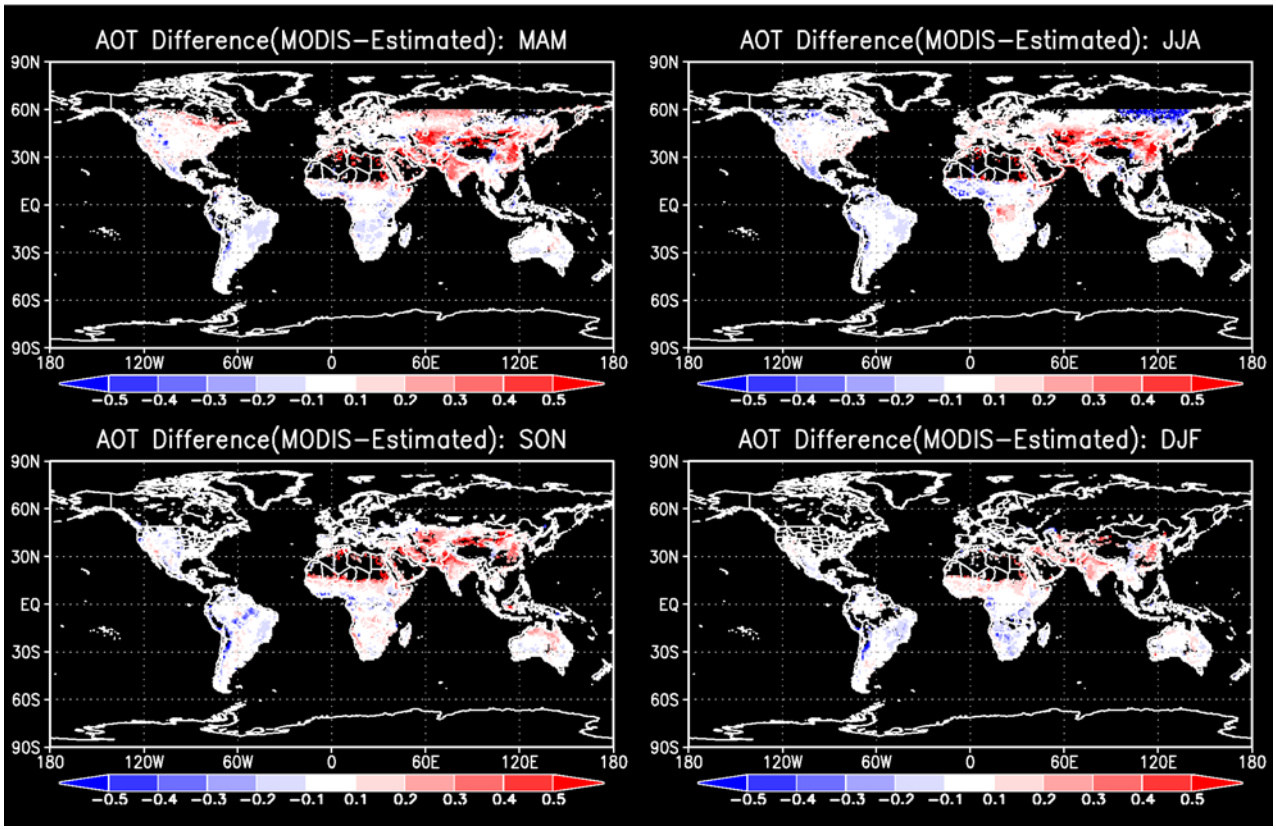


**Figure 17.** Seasonal mean difference maps between the estimated AOT over land at 0.55 μm (1983–2000) from TOMS and AVHRR data sets (as shown in Figure 15) and MODIS AOT (April 2000 to March 2004).

means. Figure 17 shows the maps of the seasonal mean differences between MODIS and the estimated AOTs over land. The two AOTs agree well with each other in general except for Asia. The primary reasons for the large disparity in Asia are likely to include (1) the fact that statistical relations between TOMS and AVHRR AOTs for heavy pollution and Asian dust were not established due to ubiquitous missing data in TOMS AOT at higher latitudes along major cloud regimes and (2) the dependence of TOMS AOT on aerosol altitude (i.e., lower altitude near the source regions). Figure 18 shows multiyear monthly averages of the two AOTs over the respective continents. On a continental scale, our AOT estimation from TOMS data shows a similar seasonality to that from MODIS. Good agreement is found in North America and Australia. For South America and Asia, systematic differences are found, but their seasonal variations track each other quite well. It is interesting to note that the MODIS AOT and our AOT estimations over South Africa cross each other before and after the peak season of biomass burning. It is difficult to pinpoint the causes, but major factors influencing the systematic differences may include: (1) systematic differences between regional mean MODIS and GACP/AVHRR AOTs as revealed in the work of *Jeong et al.* [2005], noting that the estimated AOT over land is a GACP/AVHRR-like AOT); (2) the dependence of TOMS AOT on the altitude of the aerosol layer (and topography) and aerosol absorption (single-scattering albedo), especially in the dust and biomass burning regimes; (3) differences in sampling periods, which may explain the large blue area over Russia during JJA in Figure 17. The sound agreement between the two AOTs and their seasonality suggest that AOT estimations from the past can be linked to current state-of-art AOT estimations for development of continuous long-term records.

## 5. Summary and Conclusions

[44] Global aerosol products play an important role in climate change studies due to their complex direct and indirect effects. While numerous global aerosol products have been generated from various satellite sensors, much more insight into these products is needed to understand them in terms of their strengths, weaknesses and synergies, in order to (1) make informative and creative use of the data, (2) to extract as much information as possible from the data, and (3) to filter out any inherent noise and uncertainties for future improvement in both data quality and quantity. Presented here is a preliminary study toward achieving this goal by examining the quality, compatibility and synergy between two prominent global aerosol products derived from AVHRR and TOMS [*Mishchenko et al.*, 1999; *Torres et al.*, 2002].

[45] Cloud contamination has been a common inherent problem suffered by both products [*Ignatov and Nalli*, 2002; *Myhre et al.*, 2004]. Nearly all aerosol-laden regions outside of the tropics correspond to high/frequent cloud cover. Regions of highly suspected cloud contamination include the Southern Hemispheric Oceans (30–60°S) in all

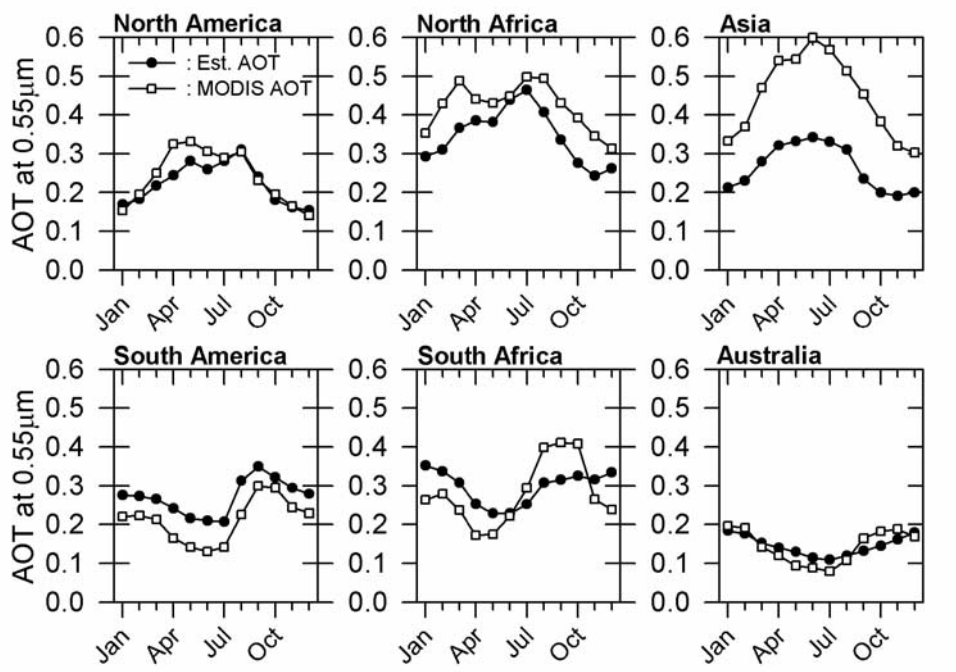


**Figure 18.** Comparison of multiyear monthly averages of the estimated AOT (1983–2000) and MODIS AOT (April 2000 to March 2004) over the continents. Note that Africa was separated at the equator into north and south regions. Each continental monthly average includes all available colocated data sets for respective continents.

the seasons and some parts of the North Pacific Oceans during JJA (and MAM but much weaker). Unfortunately, the monthly products used here convey little information to aid in comprehending the problem. However, regional analyses with aerosol physics in mind are instrumental in gaining further insight into the likely effects of cloud and other factors. In general, it seems safe to conclude that while cloud contamination contributes to AOT values to a varying degree, the general patterns of enhanced AOT appear to be true, rather than artifacts due to cloud contamination. Unraveling the various other effects remains a major challenge, which is crucial to furthering our understanding of many aerosol-related issues.

[46] To this end, attempts are made here to conduct in-depth regional analyses using a variety of data sets. The following regions were selected based on certain unique features that have not been previously addressed: off the coast of Peru, a tropical zone between western Africa to eastern central Pacific, and North Pacific regions. First, the high AOT associated with small AE off the shores of Peru is due to cloud contamination. If this were not so, the presence of small AE would contradict other studies that reported small particles in this region and argued about the apparent evidence of an aerosol indirect effect. Second, the long plumes of enhanced AOT along the equatorial eastern Pacific (EC Pacific) have a complex and interesting seasonality that is driven by atmospheric circulation. The plume is a manifestation of the convergence of various types of aerosols (dust, smoke, pollution aerosols, etc.) transported by prevailing winds that change with season. Third, the generally enhanced aerosol field over the North Pacific is found to consist primarily of fine-mode aerosols and the loading responds sharply to the changes in wind direction, signifying heavy influence by aerosols (especially pollution) transported from Asia. However, there is no discernible dust signal in terms of relative values of AE even during the dust-active season in spring. This could be due to the smearing out of sporadic dust episodes by averaging in a month or due to the misclassification of dust as cloud. However, significant correlations found between the AVHRR AOT and chlorophyll concentration around these regions suggest a possible influence of ocean color contamination and/or induced oceanic aerosols such as nss sulfate, which can be linked to phytoplankton activity.

[47] The AVHRR and TOMS aerosol products also exhibit a good synergy, which is exploited here. For example, TOMS data alone has difficulty in differentiating between dust and biomass burning aerosols, which can be compensated for by the AVHRR AE pertaining to aerosol size. Taking advantage of their respective strengths, we developed an algorithm to classify aerosol types into dust, biomass burning, a mixture of the two, sulfate/pollution, and sea salt, etc. Using this algorithm, regions under the dominant influence of various types of aerosols are determined from the two satellite products alone. Prior to MODIS and MISR, it has been difficult to gain such information from a single satellite. The performance of this algorithm is influenced by the quality of each aerosol product (especially the AVHRR AE and the TOMS AI).

[48] As an application of the classification and exploitation of the synergy, the two AOT products are integrated to generate an AOT product at a common wavelength (0.55 μm) of truly global coverage covering both ocean and land. To reduce the large scattering and biases exhibited

when direct comparisons of the two products were made, different relationships were derived between the TOMS and AVHRR AOTs according to aerosol type. The range of uncertainty of the estimated AOT is $\pm 0.08 \pm 0.20\tau$. These inferred AOTs are compared to AERONET measurements, and most of the estimations fall within this range of uncertainty. In addition, comparisons of the inferred AOTs with MODIS AOTs show good agreement in terms of magnitude and seasonality, suggesting that bridging past and current AOT estimations is promising.

[49] **Acknowledgments.** We thank the GACP team at NASA/GISS and MODIS, TOMS and AERONET teams at NASA GSFC for processing and providing the aerosol products. We are grateful to S.-C. Tsay, A. Chu, and F.-L. Chang for useful discussions. The NASA Distributed Active Archive Centers at LaRC and GSFC are acknowledged for distributing various data sets employed here. This study is supported under the following grants provided by DOE, NASA, ONR, and NSF with grants DEFG0201ER63166, NGT530475/NNG04GE79G, N0001402IP20018, and ATM0425069, respectively.

## References

Andreae, M. O., et al. (1994), Biomass burning in the global environment: First results from the IGAC/BIBEX field campaign STARE/TRACE-A/SAFARI 92, in *Global Atmospheric-Biospheric Chemistry*, edited by R. G. Prinn, pp. 83–101, Plenum, New York.

Bellouin, N., O. Boucher, D. Tanré, and O. Dubovik (2003), Aerosol absorption over the clear-sky oceans deduced from POLDER-1 and AERONET observations, *Geophys. Res. Lett.*, *30*(14), 1748, doi:10.1029/2003GL017121.

Bretherton, C. S., T. Uttal, C. W. Fairall, S. E. Yuter, R. A. Weller, D. Baumgardner, K. Comstock, R. Wood, and G. B. Raga (2004), The EPIC 2001 stratocumulus study, *Bull. Am. Meteorol. Soc.*, *85*(7), 967–977.

Cakmur, R. V., R. L. Miller, and I. Tegen (2001), A comparison of seasonal and interannual variability of soil dust aerosols over the Atlantic Ocean as inferred by the TOMS AI and AVHRR AOT retrievals, *J. Geophys. Res.*, *106*(D16), 18,287–18,303.

Charlson, R. J., J. E. Lovelock, M. O. Andreae, and S. G. Warren (1987), Oceanic phytoplankton, atmospheric sulphur, cloud albedo and climate, *Nature*, *326*, 655–661.

Chin, M., P. Ginoux, S. Kinne, O. Torres, B. N. Holben, B. N. Duncan, R. V. Martin, J. A. Logan, A. Higurashi, and T. Nakajima (2002), Tropospheric aerosol optical thickness from the GOCART model and comparisons with satellite and Sun photometer measurements, *J. Atmos. Sci.*, *59*, 461–483.

Deuzé, J. L., P. Goloub, M. Herman, A. Marchand, G. Perry, S. Susana, and D. Tanré (2000), Estimate of the aerosol properties over the ocean with POLDER, *J. Geophys. Res.*, *105*, 15,329–15,346.

Dubovik, O., B. Holben, T. F. Eck, A. Smirnov, Y. J. Kaufman, M. D. King, D. Tanré, and I. Slutsker (2002), Variability of absorption and optical properties of key aerosol types observed in worldwide locations, *J. Atmos. Sci.*, *59*, 590–608.

Eck, T. F., B. N. Holben, J. S. Reid, O. Dubovik, A. Smirnov, N. T. O'Neill, I. Slutsker, and S. Kinne (1999), Wavelength dependence of the optical depth of biomass burning, urban, and desert dust aerosols, *J. Geophys. Res.*, *104*(D24), 31,333–31,349.

Fukushima, H., and M. Toratani (1997), Asian dust aerosol: Optical effect on satellite ocean color signal and a scheme of its correction, *J. Geophys. Res.*, *102*(D14), 17,119–17,130.

Geogdzhayev, I. V., M. I. Mishchenko, W. B. Rossow, B. Cairns, and A. A. Lacis (2002), Global two-channel AVHRR retrievals of aerosol properties over the ocean for the period of NOAA-9 observations and preliminary retrievals using NOAA-7 and NOAA-11 data, *J. Atmos. Sci.*, *59*(3), 262–278.

Ginoux, P., M. Chin, I. Tegen, J. Prospero, B. Holben, D. Dubovik, and S. J. Lin (2001), Sources and distributions of dust aerosols simulated with the GOCART model, *J. Geophys. Res.*, *106*, 20,255–20,273.

Goloub, P., D. Tanré, J. L. Deuzé, M. Herman, A. Marchand, and F.-M. Breon (1999), Validation of the first algorithm applied for deriving the aerosol properties over the ocean using the POLDER/ADEOS measurements, *IEEE Trans. Geosci. Remote Sens.*, *37*, 1586–1596.

Gong, S. L., X. Y. Zhang, T. L. Zhao, I. G. McKendry, D. A. Jaffe, and N. M. Lu (2003), Characterization of soil dust aerosol in China and its transport and distribution during 2001 ACE-Asia: 2. Model simulation and validation, *J. Geophys. Res.*, *108*(D9), 4262, doi:10.1029/2002JD002633.

Gregg, W. W., M. E. Conkright, J. E. O'Reilly, F. S. Patt, M. H. Wang, J. A. Yoder, and N. W. Casey (2002), NOAA-NASA coastal zone color scanner reanalysis effort, *Appl. Opt.*, *41*(9), 1615–1628.

Haywood, J. M., P. N. Francis, I. Geogdzhayev, M. Mishchenko, and R. Frey (2001), Comparison of Saharan dust aerosol optical depths retrieved using aircraft mounted pyranometers and 2-channel AVHRR algorithms, *Geophys. Res. Lett.*, *28*(12), 2393–2396.

Herman, J. R., P. K. Bhartia, O. Torres, C. Hsu, C. Seftor, and E. Celarier (1997), Global distribution of UV-absorbing aerosols from Nimbus 7/TOMS data, *J. Geophys. Res.*, *102*(D14), 16,911–16,922.

Higurashi, A., and T. Nakajima (1999), Development of a two-channel aerosol retrieval algorithm on a global scale using NOAA AVHRR, *J. Atmos. Sci.*, *56*, 924–941.

Hobbs, P. V., P. Sinha, R. J. Yokelson, T. J. Christian, D. R. Blake, S. Gao, T. W. Kirchstetter, T. Novakov, and P. Pilewskie (2003), Evolution of gases and particles from a savanna fire in South Africa, *J. Geophys. Res.*, *108*(D13), 8485, doi:10.1029/2002JD002352.

Holben, B. N., et al. (1998), AERONET—A federated instrument network and data archive for aerosol characterization, *Remote Sens. Environ.*, *66*, 1–16.

Holben, B. N., et al. (2001), An emerging ground-based aerosol climatology: Aerosol optical depth from AERONET, *J. Geophys. Res.*, *106*(D11), 12,067–12,097.

Hsu, N. C., J. R. Herman, P. K. Bhartia, C. J. Seftor, O. Torres, A. M. Thompson, J. F. Gleason, T. F. Eck, and B. N. Holben (1996), Detection of biomass burning smoke from TOMS measurements, *Geophys. Res. Lett.*, *23*(7), 745–748.

Hsu, N. C., J. R. Herman, O. Torres, J. F. Gleason, O. Torres, and C. J. Seftor (1999a), Satellite detection of smoke aerosols over a snow/ice surface by TOMS, *Geophys. Res. Lett.*, *26*(8), 1165–1168.

Hsu, N. C., J. R. Herman, O. Torres, B. N. Holben, D. Tanré, T. F. Eck, A. Smirnov, B. Chatenet, and F. Lavenu (1999b), Comparisons of the TOMS aerosol index with sun-photometer aerosol optical thickness: Results and applications, *J. Geophys. Res.*, *104*(D6), 6269–6279.

Husar, R. B., J. M. Prospero, and L. L. Stowe (1997), Characterization of tropospheric aerosols over the oceans with the NOAA advanced very high resolution radiometer optical thickness operational product, *J. Geophys. Res.*, *102*, 16,889–16,909.

Husar, R. B., et al. (2001), Asian dust events of April 1998, *J. Geophys. Res.*, *106*(D16), 18,317–18,330.

Ignatov, A. (2002), Sensitivity and information content of aerosol retrievals from AVHRR: Radiometric factors, *Appl. Opt.*, *41*, 991–1011.

Ignatov, A., and N. R. Nalli (2002), Aerosol retrievals from multi-year multi-satellite AVHR Pathfinder Atmosphere (PATMOS) dataset for correcting remotely sensed sea surface temperatures, *J. Atmos. Oceanic Technol.*, *19*, 1986–2008.

Ignatov, A., and L. Stowe (2000), Physical basis, premises, and self-consistency checks of aerosol retrievals from TRMM VIRS, *J. Appl. Meteorol.*, *39*, 2259–2277.

Ignatov, A., and L. Stowe (2002a), Aerosol retrievals from individual AVHRR channels. part I: Retrieval algorithm and transition from Dave to 6S radiative transfer model, *J. Atmos. Sci.*, *59*, 313–334.

Ignatov, A., and L. Stowe (2002b), Aerosol retrievals from individual AVHRR channels. part II: Quality control, probability distribution functions, information content, and consistency checks of retrievals, *J. Atmos. Sci.*, *59*, 335–362.

Ignatov, A., L. Stowe, S. Sakerin, and G. Korotaev (1995), Validation of the NOAA/NESDIS satellite aerosol product over the North Atlantic in 1989, *J. Geophys. Res.*, *100*(D3), 5123–5132.

Ignatov, A., L. Stowe, and R. Singh (1998), Sensitivity study of the Ångström exponent derived from AVHRR over oceans, *Adv. Space Res.*, *21*, 439–442.

Ignatov, A., J. Sapper, S. Cox, I. Laszlo, N. R. Nalli, and K. B. Kidwell (2004), Operational aerosol observations (AEROBS) from AVHRR/3 on board NOAA-KLM satellites, *J. Atmos. Oceanic Technol.*, *21*, 3–25.

Intergovernmental Panel on Climate Change (IPCC) (2001), *Climate Change 2001: The Scientific Basis*, Cambridge Univ. Press, New York.

Jeong, M.-J., Z. Li, D. A. Chu, and S.-C. Tsay (2005), Quality and compatibility analyses of global aerosol products derived from the advanced very high resolution radiometer and Moderate Resolution Imaging Spectroradiometer, *J. Geophys. Res.*, *110*, D10S09, doi:10.1029/2004JD004648.

Kahn, R., P. Banerjee, D. McDonald, and D. Diner (1998), Sensitivity of multiangle imaging to aerosol optical depth, and to pure-particle size distribution and composition over ocean, *J. Geophys. Res.*, *103*, 32,195–32,213.

Kahn, R., P. Banerjee, and D. McDonald (2001), Sensitivity of multiangle imaging to natural mixtures of aerosols over ocean, *J. Geophys. Res.*, *106*(D16), 18,219–18,238.

Kaufman, Y. J., D. Tanré, L. A. Remer, E. F. Vermote, A. Chu, and B. N. Holben (1997), Operational remote sensing of tropospheric aerosol over land from EOS moderate resolution imaging spectroradiometer, *J. Geophys. Res.*, *102*(D14), 17,051–17,067.

Kaufman, Y. J., D. Tanré, and O. Boucher (2002), A satellite view of aerosols in the climate system, *Nature*, *419*, 215–223.

King, M. D., Y. Kaufman, D. Tanré, and T. Nakajima (1999), Remote sensing of tropospheric aerosols from space: Past, present, and future, *Bull. Am. Meteorol. Soc.*, *11*, 2229–2259.

Kinne, S., et al. (2001), How well do aerosol retrievals from satellites and representation in global circulation models match ground-based AERONET aerosol statistics?, in *Remote Sensing and Climate Modeling: Synergies and Limitations*, edited by M. Beniston and M. M. Verstraete, pp. 103–158, Springer, New York.

Kuang, Z., and Y. L. Yung (2000), Reflectivity variations off the Peru Coast: Evidence for indirect effect of anthropogenic sulfate aerosols on clouds, *Geophys. Res. Lett.*, *27*(16), 2501–2504.

Li, Z., and L. Moreau (1996), A new approach for remote sensing of canopy-absorbed photosynthetically active radiation. I: Total surface absorption, *Remote Sens. Environ.*, *55*, 175–191.

Martonchik, J. V., D. J. Diner, R. Kahn, M. M. Verstraete, B. Pinty, H. R. Gordon, and T. P. Ackerman (1998), Techniques for the retrieval of aerosol properties over land and ocean using multiangle imaging, *IEEE Trans. Geosci. Remote Sens.*, *36*, 1212–1227.

Masuda, K., H. G. Leighton, and Z. Li (1995), A new parameterization for the determination of solar flux absorbed at the surface from satellite measurements, *J. Clim.*, *8*, 1615–1629.

Meeson, B. W., F. E. Corprew, J. M. P. McManus, D. M. Myers, J. W. Closs, K.-J. Sun, D. J. Sunday, and P. J. Sellers (1995), *ISLSCP Initiative I-Global Data Sets for Land-Atmosphere Models, 1987–1988* [CD-ROM], vol. 1–5, NASA, Greenbelt, Md.

Mishchenko, M. I., A. A. Lacis, B. E. Carlson, and L. D. Travis (1995), Nonsphericity of dust-like tropospheric aerosols: Implications for aerosol remote sensing and climate modeling, *Geophys. Res. Lett.*, *22*, 1077–1080.

Mishchenko, M. I., I. V. Geogdzhayev, B. Cairns, W. B. Rossow, and A. A. Lacis (1999), Aerosol retrievals over the ocean by use of channels 1 and 2 AVHRR data: Sensitivity analysis and preliminary results, *Appl. Opt.*, *38*, 7325–7341.

Mishchenko, M. I., I. V. Geogdzhayev, L. Liu, J. A. Ogren, A. A. Lacis, W. B. Rossow, J. W. Hovenier, H. Volten, and O. Munoz (2003), Aerosol retrievals from AVHRR radiances: Effects of particle nonsphericity and absorption and an updated long-term global climatology of aerosol properties, *J. Quant. Spectrosc. Radiat. Transfer*, *79-80*, 953–972.

Murphy, D. M., J. R. Anderson, P. K. Quinn, L. M. McInnes, F. J. Brechtel, S. M. Kreidenweis, A. M. Middlebrook, M. Posfai, D. S. Thomson, and P. R. Buseck (1998), Influence of sea-salt on aerosol radiative properties in the Southern Ocean marine boundary layer, *Nature*, *392*, 62–65.

Myhre, G., et al. (2004), Intercomparison of satellite retrieved aerosol optical depth over ocean, *J. Atmos. Sci.*, *61*, 499–513.

Nakajima, T., and A. Higurashi (1998), A use of two-channel radiances for an aerosol characterization from space, *Geophys. Res. Lett.*, *25*(20), 3815–3818.

Nakajima, T., M. Tanaka, M. Yamano, M. Siobara, K. Arao, and Y. Nakanishi (1989), Aerosol optical characteristics in the yellow sand events observed in May 1982 at Nagasaki: Part II models, *J. Meteorol. Soc. Jpn.*, *67*, 279–291.

Penner, J. E., et al. (2002), A comparison of model- and satellite-derived aerosol optical depth and reflectivity, *J. Atmos. Sci.*, *59*, 441–460.

Prospero, J. M., and L. S. Savoie (1989), Effect of continental sources on nitrate concentration over the Pacific Oceans, *Nature*, *339*, 687–689.

Prospero, J. M., D. L. Savoie, and R. Arimoto (2003), Long term record of nss-sulfate and nitrate in aerosols on Midway Island, 1981–2000: Evidence of increased (now decreasing?) anthropogenic emissions from Asia, *J. Geophys. Res.*, *108*(D1), 4019, doi:10.1029/2001JD001524.

Rao, C. R. N., L. Stowe, and P. McClain (1989), Remote sensing of aerosols over oceans using AVHRR data: Theory, practice and applications, *Int. J. Remote Sens.*, *10*, 743–749.

Remer, L. A., Y. J. Kaufman, B. N. Holben, A. M. Thompson, and D. McNamara (1998), Biomass burning aerosol size distribution and modeled optical properties, *J. Geophys. Res.*, *103*(D24), 31,879–31,891.

Rossow, W. B., and L. C. Garder (1993), Cloud detection using satellite measurements of infrared and visible radiances for ISCCP, *J. Clim.*, *6*, 2341–2369.

Rossow, W. B., and R. A. Schiffer (1999), Advances in understanding clouds from ISCCP, *Bull. Am. Meteorol. Soc.*, *80*, 2261–2287.

Siegel, D. A., M. Wang, S. Maritorena, and W. Robinson (2000), Atmospheric correction of satellite ocean color imagery: The black pixel assumption, *Appl. Opt.*, *39*, 3582–3591.

Stowe, L. L., A. M. Ignatov, and R. R. Singh (1997), Development, validation, and potential enhancements to the second-generation operational aerosol product at the National Environmental Satellite, Data, and Information Service of the National Oceanic and Atmospheric Administration, *J. Geophys. Res.*, *102*, 16,923–16,934.

Stowe, L. L., H. Jacobowitz, G. Ohring, K. R. Knapp, and N. R. Nalli (2002), The advanced very high resolution radiometer (AVHRR) Pathfinder Atmosphere (PATMOS) climate dataset: Initial analyses and evaluations, *J. Clim.*, *15*, 1243–1260.

Tanré, D., Y. J. Kaufman, M. Herman, and S. Mattoo (1997), Remote sensing of aerosol properties over oceans using the MODIS/EOS spectral radiances, *J. Geophys. Res.*, *102*(D14), 16,971–16,988.

Tanré, D., Y. J. Kaufman, B. N. Holben, B. Chatenet, A. Karneli, F. Lavenu, L. Blarel, O. Dubovik, L. A. Remer, and A. Smirnov (2001), Climatology of dust aerosol size distribution and optical properties derived from remotely sensed data in the solar spectrum, *J. Geophys. Res.*, *106*(D16), 18,205–18,217.

Tegen, I., P. Hollrig, M. Chin, I. Fung, D. Jacob, and J. Penner (1997), Contribution of different aerosol species to the global aerosol extinction optical thickness: Estimates from model results, *J. Geophys. Res.*, *102*(D20), 23,895–23,915.

Torres, O., P. K. Bhartia, J. R. Herman, Z. Ahmad, and J. Gleason (1998), Derivation of aerosol properties from satellite measurements of backscattered ultraviolet radiation: Theoretical basis, *J. Geophys. Res.*, *103*(D14), 17,099–17,110.

Torres, O., P. K. Bhartia, J. R. Herman, A. Sinyuk, P. Ginoux, and B. Holben (2002), A long-term record of aerosol optical depth from TOMS observations and comparison to AERONET measurements, *J. Atmos. Sci.*, *59*, 398–413.

van de Hulst, H. C. (1957), *Light Scattering by Small Particles*, 470 pp., John Wiley, Hoboken, N. J.

Yu, H., R. E. Dickinson, M. Chin, Y. J. Kaufman, B. N. Holben, I. V. Geogdzhayev, and M. I. Mishchenko (2003), Annual cycle of global distributions of aerosol optical depth from integration of MODIS retrievals and GOCART model simulations, *J. Geophys. Res.*, *108*(D3), 4128, doi:10.1029/2002JD002717.

Zhang, X. Y., S. L. Gong, Z. X. Shen, F. M. Mei, X. X. Xi, L. C. Liu, Z. J. Zhou, D. Wang, Y. Q. Wang, and Y. Cheng (2003), Characterization of soil dust aerosol in China and its transport and distribution during 2001 ACE-Asia: 1. Network observations, *J. Geophys. Res.*, *108*(D9), 4261, doi:10.1029/2002JD002632.

Zhao, T. X.-P., I. Laszlo, O. Dubovik, B. N. Holben, J. Sapper, D. Tanré, and C. Pietras (2003), A study of the effect of non-spherical dust particles on the AVHRR aerosol optical thickness retrievals, *Geophys. Res. Lett.*, *30*(6), 1317, doi:10.1029/2002GL016379.

Zhou, J., E. Swielicki, H. C. Hansson, and P. Artaxo (2002), Submicrometer aerosol particle size distribution and hygroscopic growth measured in the Amazon rain forest during the wet season, *J. Geophys. Res.*, *107*(D20), 8055, doi:10.1029/2000JD000203.

M.-J. Jeong and Z. Li, Department of Meteorology and Earth System Science Interdisciplinary Center, University of Maryland, 2207 CSS Building, College Park, MD 20742-2465, USA. (mjeong@atmos.umd.edu; zli@atmos.umd.edu)